UNIVERSITY OF AMSTERDAM

UvA-DARE (Digital Academic Repository)

# Contrasting nutritional strategies in two closely related marine mixotrophic chrysophytes

Wilken, S.; Choi, C.J.; Worden, A.Z.

**DOI**
10.1111/jpy.12920

**Publication date**
2020

**Document Version**
Final published version

**Published in**
Journal of phycology

**License**
CC BY

Link to publication

**Citation for published version (APA):**
Wilken, S., Choi, C. J., & Worden, A. Z. (2020). Contrasting nutritional strategies in two closely related marine mixotrophic chrysophytes. *Journal of phycology*, *56*(1), 52-67. https://doi.org/10.1111/jpy.12920

**General rights**
It is not permitted to download or to forward/distribute the text or part of it without the consent of the author(s) and/or copyright holder(s), other than for strictly personal, individual use, unless the work is under an open content license (like Creative Commons).

**Disclaimer/Complaints regulations**
If you believe that digital publication of certain material infringes any of your rights or (privacy) interests, please let the Library know, stating your reasons. In case of a legitimate complaint, the Library will make the material inaccessible and/or remove it from the website. Please Ask the Library: https://uba.uva.nl/en/contact, or a letter to: Library of the University of Amsterdam, Secretariat, P.O. Box 19185, 1000 GD Amsterdam, The Netherlands. You will be contacted as soon as possible.

*UvA-DARE is a service provided by the library of the University of Amsterdam (https://dare.uva.nl)*

Download date:05 Sept 2026

*J. Phycol.* **56,** 52–67 (2020)
© 2019 The Authors. *Journal of Phycology* published by Wiley Periodicals, Inc. on behalf of Phycological Society of America.
This is an open access article under the terms of the Creative Commons Attribution License, which permits use, distribution and reproduction in any medium, provided the original work is properly cited.
DOI: 10.1111/jpy.12920

# CONTRASTING MIXOTROPHIC LIFESTYLES REVEAL DIFFERENT ECOLOGICAL NICHES IN TWO CLOSELY RELATED MARINE PROTISTS[1]

*Susanne Wilken*[2]

Monterey Bay Aquarium Research Institute, 7700 Sandholdt Road, Moss Landing, California 95039, USA
Department of Freshwater and Marine Ecology, Institute for Biodiversity and Ecosystem Dynamics, University of Amsterdam, Science Park 904, Amsterdam 1098 XH, The Netherlands

*Chang Jae Choi, and Alexandra Z. Worden*[2]

Monterey Bay Aquarium Research Institute, 7700 Sandholdt Road, Moss Landing, California 95039, USA
Ocean EcoSystems Biology Unit, GEOMAR Helmholtz Centre for Ocean Research, Düsternbrooker Weg 20, Kiel 24105, Germany

**Many marine microbial eukaryotes combine photosynthetic with phagotrophic nutrition, but incomplete understanding of such mixotrophic protists, their functional diversity, and underlying physiological mechanisms limits the assessment and modeling of their roles in present and future ocean ecosystems. We developed an experimental system to study responses of mixotrophic protists to availability of living prey and light, and used it to characterize contrasting physiological strategies in two stramenopiles in the genus *Ochromonas*. We show that oceanic isolate CCMP1393 is an obligate mixotroph, requiring both light and prey as complementary resources. Interdependence of photosynthesis and heterotrophy in CCMP1393 comprises a significant role of mitochondrial respiration in photosynthetic electron transport. In contrast, coastal isolate CCMP2951 is a facultative mixotroph that can substitute photosynthesis by phagotrophy and hence grow purely heterotrophically in darkness. In contrast to CCMP1393, CCMP2951 also exhibits a marked photoprotection response that integrates non-photochemical quenching and mitochondrial respiration as electron sink for photosynthetically produced reducing equivalents. Facultative mixotrophs similar to CCMP2951 might be well adapted to variable environments, while obligate mixotrophs similar to CCMP1393 appear capable of resource efficient growth in oligotrophic ocean environments. Thus, the responses of these phylogenetically close protists to the availability of different resources reveals niche differentiation that influences impacts in food webs and leads to opposing carbon cycle roles.**

*Key index words:* **chrysophytes; microbial food web; mixotrophy; phagotrophy; phytoplankton**

***Abbreviations*: AOX, mitochondrial alternative oxidase; ASW, artificial seawater; $C_{III}$, mitochondrial respiratory complex III; ETR, electron transport rate; FALS, forward-angle light scatter; FISH, fluorescence in situ hybridization; FRRf, Fast repetition rate fluorometry; GFP, green fluorescent protein; NPQ, non-photochemical quenching; PTOX, plastid terminal oxidase; VAZ, violaxanthin cycle pigments**

Unicellular photosynthetic eukaryotes of diverse evolutionary origin have long been recognized as globally important primary producers in the ocean (Field et al. 1998). As phytoplankton, these pigmented protists are clearly distinguished from purely heterotrophic protists, which are considered the major predators in marine microbial food webs, recycling nutrients, and linking bacterial production to higher trophic levels (Pomeroy 1974, Azam et al. 1983). However, this strict dichotomy does not accurately reflect natural communities, which harbor many mixotrophic protists that combine the ability to photosynthesize with phagotrophic consumption of microbial cells (Bird and Kalff 1986, Estep et al. 1986, Flynn et al. 2013). Mixotrophs can be important consumers of prokaryotic and eukaryotic microbes (Havskum and Hansen 1997, Sanders et al. 2000, Unrein et al. 2007, Hartmann et al. 2012, Orsi et al. 2018), but their concurrent contributions to carbon fixation via photosynthesis complicate integration of their ecosystem roles into biogeochemical models (Mitra et al. 2014, Worden et al. 2015). When both processes are integrated within the same cell, photosynthetic energy acquisition can compensate respirational losses of ingested carbon (Stoecker and Michaels 1991) leading to higher carbon transfer efficiencies from prey to predator, which is predicted to result in more

[1]Received 14 February 2019. Accepted 13 August 2019. First Published Online 16 September 2019. Published Online 1 November 2019, Wiley Online Library (wileyonlinelibrary.com).
[2]Authors for correspondence: s.wilken@uva.nl; azworden@geomar.de
Editorial Responsibility: T. Mock (Associate Editor)

productive food chains (Ward and Follows 2016). Concurrently, higher trophic transfer efficiencies result in lesser release of remineralized nutrients by mixotrophic compared to heterotrophic predators (Rothhaupt 1997). However, the net impact of phagotrophic mixotrophs on carbon cycling may vary widely between species or environmental conditions, creating considerable uncertainty in how these organisms should be included in ecosystem models. The accuracy of theory-based predictions that involve mixotrophy, such as trait-based approaches (Andersen et al. 2015) or detailed physiological models (Flynn and Mitra 2009), is currently limited by the weak empirical basis for model assumptions and parameterization.

The combined capacity for photosynthesis and phagocytosis in many extant eukaryotes is not surprising. Phagocytosis is an ancient trait that has been involved in acquiring photosynthetic cells as endosymbionts, giving rise to the first eukaryotic photosynthetic organelle, the plastid, and then spreading into evolutionarily distant lineages of eukaryotes through additional endosymbiosis events (Lane and Archibald 2008, Keeling et al. 2013, Worden et al. 2015). In some photosynthetic eukaryotes, the capacity for phagocytosis has been lost, such as diatoms, which belong to the stramenopiles. However, the presence of mixotrophs across distant branches of the eukaryotic tree (such as multiple independent lineages within the alveolates, prymnesiophytes, and stramenopiles), with different evolutionary histories, cellular morphologies, and metabolic potentials, suggests that plastid acquisition does not necessarily result in evolution toward specialist photoautotrophy (Selosse et al. 2017). Despite the phylogenetic diversity among mixotrophs their lifestyles can be classified functionally into non-constitutive mixotrophs that acquire their photosynthetic potential by hosting photosynthetic endosymbionts or stealing plastids, and constitutive mixotrophs that possess their own plastids (Mitra et al. 2016). Additionally, mixotrophic strategies vary in the degree to which photoautotrophy and phago-heterotrophy contribute to the overall nutrition (Stoecker 1998) and the phenotypic plasticity that allows adjusting the strategy in response to environmental conditions. Recent attempts have started to address this functional diversity of mixotrophs in models (Flynn and Mitra 2009, Mitra et al. 2016, Berge et al. 2017, Leles et al. 2018), but underlying metabolic attributes will need to be resolved to understand the biogeochemical and ecological impact as well as evolutionary trajectories of photosynthetic eukaryotes.

The taxonomic identity of the plastid-containing constitutive mixotrophs that often dominate bacterivory in marine environments is not well characterized and studies quantifying their impact rarely report community composition (but see Unrein et al. 2014). Multiple prymnesiophytes and a specific group within the stramenopiles, the chrysophytes, have been identified as mixotrophic bacterivores in oligotrophic ocean regions (Hartmann et al. 2013). The few studies that have evaluated chrysophyte abundances, either by enumeration of plastid-containing chrysophytes using FISH (Jardillier et al. 2010) or by semi-quantitative dot-blot hybridization (Lepère et al. 2009, Kirkham et al. 2013), identified them as a numerically important component of pico- and nanophytoplankton communities in the tropical North-East Atlantic, the hyper-oligotrophic South Pacific gyre, the Arctic and Indian oceans. Chrysophyte sequences retrieved from environmental assays are typically dominated by environmental clades (Lepère et al. 2009, del Campo and Massana 2011), and the roles of individual clades in the marine microbial food web remain unknown. Chrysophytes include species with numerous nutritional strategies from autotrophic to various mixotrophic and purely heterotrophic lifestyles, with loss of photosynthetic capabilities having occurred multiple times independently (Boenigk et al. 2005, Grossmann et al. 2016). However, physiological information for this group is largely based on cultured isolates from freshwater (Caron et al. 1990, Rothhaupt 1996), brackish, and coastal environments (Andersson et al. 1989, Flöder et al. 2006). It is unclear how far information from coastal isolates or other evolutionarily distant groups such as dinoflagellates can be extrapolated to oceanic chrysophytes. The sole study of an oceanic chrysophyte, *Ochromonas* CCMP1393, uses transcriptome analyses to infer that it has a stronger dependence on photosynthesis than a freshwater isolate (Lie et al. 2018). Mixotrophic strategies observed in freshwater and brackish *Ochromonas* species often show a strong heterotrophic component with the ability to grow purely heterotrophically in darkness (Tittel et al. 2003, Pålsson and Daniel 2004). A close interaction between photosynthetic and mitochondrial electron flow as also known from diatoms (Allen et al. 2008, Bailleul et al. 2015) has been hypothesized to underlie a tendency toward photoheterotrophy in the freshwater *O. danica* (Wilken et al. 2014a). However, *Ochromona*s as defined today appears to be polyphyletic (Grossmann et al. 2016) and the physiology of marine isolates has yet to be directly compared in feeding experiments.

The nutritional diversity of chrysophytes provides a platform for investigating differentiated strategies in phylogenetically related organisms from various environments. The challenges to studying energetics and implications of different mixotrophic strategies lie principally in the maintenance of predatory mixotrophs in culture under axenic conditions and performing experiments with living prey. While mesocosm studies have employed bacteria expressing green fluorescent protein (GFP) as experimental amendments of traceable living prey (Worden et al. 2006), this approach has yet to be employed

in culture-based studies. Here we developed a controlled experimental system to manipulate and track the availability of live bacterial prey, using a marine *Vibrio* mutant that has a higher temperature optimum (Graf et al. 1994) than the eukaryotes under study and harbors GFP on an antibiotic resistance plasmid. These systems were developed for two marine chrysophytes expected to represent different species, the coastal (CCMP2951) and oceanic (CCMP1393) *Ochromonas* isolates. We compared the relative importance of photosynthesis and ingestion of bacterial prey to nutrition of both isolates and assessed the phenotypic plasticity in response to variations in light intensity and prey availability. To examine differences in their lifestyles more deeply, we further tested for a potential interaction between nutritional pathways, by assessing the role of mitochondrial respiration in photosynthetic electron transport. Our study provides first insights into the underlying metabolic and physiological characteristics of distinct nutritional strategies in predatory mixotrophs from both coastal and oceanic environments. Collectively, such studies will improve our ability to mechanistically integrate widespread mixotrophic lifestyles into models used to predict carbon cycling under future ocean conditions.

## MATERIALS AND METHODS

*Chrysophyte isolates and growth conditions.* The two *Ochromonas* isolates, CCMP1393 and CCMP2951, were obtained from the National Center for Marine Algae and Microbiota (NCMA, East Boothbay, ME, USA). They originate from the North-West Atlantic Gulf Stream (38.70° N, 72.37° W) and a coastal site in the subtropical North-West Pacific (24.76° N, 125.44° E), respectively. Morphological differences indicate that they might represent different species with an eyespot being present in CCMP2951 (as documented on the NCMA website: https://ncma.bigelow.org/ccmp2951#.XNvQzcTgpPY) but not CCMP1393. The cultures were grown on K-medium containing both ammonium (50 μM) and nitrate (882 μM) as nitrogen source and $Na_2$-glycerophosphate (10 μM) as phosphorus source (Keller et al. 1987) in an artificial seawater (ASW) base with a salinity of 34. This medium was chosen because it had been developed specifically for oceanic microalgae and because the presence of ammonium and glycerophosphate would prevent impaired photosynthetic growth of *Ochromonas* due to potential inaccessibility of standard inorganic nutrient sources such as nitrate (Wilken et al. 2014b). However, we note the possibility of the organic phosphorus source to also support low levels of osmotrophy. Cultures received additions of heat-killed bacterial prey (see below) and were maintained at 21°C on a 14:10 h light:dark cycle with a light intensity of 100 μmol photons $\cdot$ $m^{-2}$ $\cdot$ $s^{-1}$ unless indicated otherwise.

*Development of controlled prey experimental system.* The two chrysophytes were rendered axenic by killing their undefined bacterial consortia using antibiotics. Specifically, they were incubated with 8 μg $\cdot$ $mL^{-1}$ chloramphenicol for 24 h, transferred into medium containing 40 μg $\cdot$ $mL^{-1}$ kanamycin, 80 μg $\cdot$ $mL^{-1}$ neomycin, 100 μg $\cdot$ $mL^{-1}$ streptomycin, and 150 μg $\cdot$ $mL^{-1}$ penicillin G, and grown in this antibiotic cocktail with transfer and feeding with heat-killed bacterial prey (see below) every other day for a total of 2 weeks. Success of the antibiotic treatment was verified by testing for bacterial growth in a medium containing peptone and malt extract, and by epifluorescence microscopy based on staining with 15 nM 4′,6-Diamidine-2′-phenylindole dihydrochloride (DAPI).

The non-motile FlrA-mutant of *Vibrio fischeri* ES114 (Millikan and Ruby 2003) was used as both a heat-killed bacterial prey source and a traceable living food source. Introduction of the pVSV102 plasmid further conferred kanamycin resistance and constitutive expression of GFP (Dunn et al. 2006). Stock cultures of the mutant were maintained on LBS plates (Stabb et al. 2001) with 100 μg $\cdot$ $mL^{-1}$ kanamycin at room temperature. Prior to experiments, *V. fischeri* was transferred into liquid medium containing 100 μM phosphate, 821 μM ammonium chloride, 888 μM glucose, K-medium trace metal mix (Keller et al. 1987), 4 mM Tris HCl pH 7.5, and 100 μg $\cdot$ $mL^{-1}$ kanamycin in an ASW base. Bacteria were harvested in exponential phase (abundance between 0.8 and 1.3 $\times$ $10^9$ cells $\cdot$ $mL^{-1}$) and either heat-killed at 80°C for 30 min (for maintenance of chrysophyte stock cultures) or used as live bacterial prey for experiments. Bacterial cells were centrifuged at 10,000*g* for 12 min, washed in KASW medium, and stored at 4°C overnight prior to use in experiments.

*Flow cytometry.* Cells were enumerated by flow cytometry after fixation with freshly prepared, buffered formaldehyde (pH 7.2; 1% final concentration) and dark incubation for 20 min. Fixation in this manner did not induce visible prey egestion. Fixed samples were either run immediately on an Accuri C6 flow cytometer (BD Biosciences, San Jose, CA, USA) or flash-frozen in liquid nitrogen and stored at −80°C until analysis on an Influx flow cytometer (BD Biosciences; for details see: Cuvelier et al. 2010). Red and yellow-green polystyrene fluorescent beads (Polysciences, Warrington, PA, USA) were added as internal standards. On the Accuri, the detection threshold was set on forward-angle light scatter (FALS) for *Ochromonas* and on green fluorescence (510/15 nm) for *V. fischeri*. For the latter, settings were validated against flow-cytometric bacterial counts after DNA staining with SybrGreen (Invitrogen), to ensure that the GFP signal was sufficient to detect all bacteria. The chlorophyll-derived autofluorescence of *Ochromonas* cells was normalized to the red beads and represents a proxy for chlorophyll content (Cuvelier et al. 2017).

*DNA extraction, sequencing, and phylogenetic analyses.* CCMP2951 cells were harvested from 50 mL culture by centrifugation at 8,000*g* for 10 min. DNA was extracted using the DNeasy Plant Mini Kit (Qiagen, Valencia, CA, USA). Polymerase chain reaction (PCR) to amplify the 18S rRNA gene was performed using forward primer 5′-ACCTGGTTGATCCTGCCAG-3′ and reverse primer 5′-TGATCCTTCYGCAGGTTCAC-3′ (Moon-van der Staay et al. 2000) in a total volume of 25 μL containing 0.2 μM of each primer, 1 μL template, and 12.5 μL of HotStarTaq MasterMix (Qiagen). After initial activation at 95°C for 15 min, 30 amplification cycles were performed consisting of 30 s at 95°C, 30 s at 50°C, 4 min at 72°C, followed by 10 min final extension at 72°C. PCR products were purified by electrophoresis, gel extracted (QIAquick Gel Extraction Kit; Qiagen), and cloned with the TOPO-TA cloning kit (Invitrogen, Carlsbad, CA, USA). Plasmids were Sanger-sequenced bi-directionally using plasmid primers M13F/M13R and the two internal primers 502f and 1174r (Worden 2006). The resulting 1,786 bp CCMP2951 18S rRNA gene sequence was deposited under accession MH420530 (NCBI NR).

Near full-length 18S rRNA gene sequences representing chrysophyte diversity were retrieved from the SILVA database (release 128, https://www.arb-silva.de/documentation/release-128/; Pruesse et al. 2007). These 126 sequences, 4 additional sequences retrieved from iMicrobe MMETSP database

(Keeling et al. 2014), alongside the CCMP2951 sequence generated herein and a Synchromophyceae sequence (as outgroup) were aligned using MAFFT (Katoh and Standley 2013) with default parameters. Gaps were masked using Gblocks (Castresana 2000) and phylogenetic inferences made by maximum likelihood methods based on 1,444 homologous positions implemented in RAxML (Stamatakis 2014) under the gamma corrected GTR model of evolution with 1,000 bootstrap replicates, or PhyML 3.0.1 (Guindon et al. 2010) with the same substitution model and 100 bootstrap replicates. Additional reconstructions were performed in MrBayes 3.2.6 (Ronquist et al. 2012) and the final tree was produced using FigTree 1.4.0 (http://tree.bio.ed.ac.uk/software/figtree) and RAxML topology. Literature searches were performed for all genera represented in the tree to retrieve information on their capabilities to perform photosynthesis and phagocytosis. We note that detection of phagotrophic capacity requires a targeted experiment while photosynthetic capacity is inferred from readily detectable pigmentation of cells.

*Experiments*. Prior to experiments, the *Ochromonas* isolates were acclimated to experimental conditions by maintenance in semi-continuous culture for 10 generations with both light and prey being available. To achieve this, cell abundances were kept between 5 and $10 \times 10^4$ cells $\cdot$ mL$^{-1}$ and live bacterial prey was added daily to an abundance of $3 \times 10^7$ cells $\cdot$ mL$^{-1}$. These abundances were established in preliminary feeding experiments to avoid prey depletion to sub-saturating abundances below $1 \times 10^7$ cells $\cdot$ mL$^{-1}$ within 24 h (Rothhaupt 1996), but allow depletion of prey by three orders of magnitude over a longer period (3 d). Daily dilution of cultures with fresh medium and supplementation of live bacterial prey was based on flow cytometry counts of both predator and prey.

Three experiments were performed using the GFP traceable, live bacterial prey. Experiment 1 addressed the growth response to light intensity under mixotrophic conditions (with prey-amendment), Experiment 2 addressed the growth response to availability of light and prey, and Experiment 3 assessed physiological responses to light limitation and prey depletion.

For Experiment 1, light–response curves were performed in triplicate for both isolates under prey-amended conditions. The light intensities used examined the same range of light levels, with slight differences in specific levels between isolate experiments, with CCMP1393 grown at 0, 15, 30, 80, 130, and 210 μmol photons $\cdot$ m$^{-2}$ $\cdot$ s$^{-1}$ and CCMP2951 at 0, 20, 40, 57, 95, and 165 μmol photons $\cdot$ m$^{-2}$ $\cdot$ s$^{-1}$. Cells were enumerated daily by flow cytometry (Accuri C6) as described above. Biological triplicates of each isolate were maintained for 10 generations and specific growth rates were then averaged over the last 5 d of the growth period for each biological replicate.

Experiment 2 further assessed the potential for purely autotrophic or heterotrophic growth. To this end, triplicate cultures of both isolates were pre-grown mixotrophically with daily prey-amendments (as described above) at a light intensity of 100 μmol photons $\cdot$ m$^{-2}$ $\cdot$ s$^{-1}$, close to the optimum determined for each isolate (see results). Cultures were then split into (i) an autotrophic treatment that did not receive additional prey; (ii) a mixotrophic treatment that continued to receive daily prey-amendments; and (iii) a heterotrophic treatment that received daily prey-amendments, but was kept in darkness. Cultures were maintained for 7 d as described above, sampled daily, and enumerated by flow cytometry.

For Experiment 3, triplicate cultures of both isolates were acclimated to limiting (low) light intensity of 15 or near-optimal (high) light intensity of 100 μmol photons $\cdot$ m$^{-2}$ $\cdot$ s$^{-1}$, respectively, and maintained for 10 generations as described above. Cultures were then split into a mixotrophic, prey-amended treatment grown with continued addition of bacterial prey as before and a prey-deplete treatment that did not receive additional prey. Both treatments were grown semi-continuously for four more days with daily sampling for flow cytometry and dilution to $5 \times 10^4$ cells $\cdot$ mL$^{-1}$. Photo-physiological sampling and measurements were performed after 3 d, when both isolates still exhibited positive growth rates when receiving sufficient light (i.e., 100 μmol photons $\cdot$ m$^{-2}$ $\cdot$ s$^{-1}$), while afterwards CCMP2951 ceased growing in prey-deplete treatments. This experiment thus assessed the short-term response to prey depletion rather than acclimated autotrophic growth, which the two isolates were not capable of. Samples were taken for pigment analysis and measurements of both carbon fixation and prey ingestion rates. Fast repetition rate fluorometry (FRRf) was used to record rapid light–response curves and the response of photosynthetic electron transport to chemical inhibition of mitochondrial respiration or chlororespiration.

*Pigment analysis*: For pigment analysis, 50 mL of culture was filtered onto 25-mm GF/F filters (Whatman, GE Healthcare Life Sciences, Pittsburgh, PA, USA), frozen in liquid $N_2$, and stored at −80°C. Extraction and HPLC analysis were performed at the analytical facility of Horn Point Laboratory at the University of Maryland Center for Environmental Science. Concentrations of chlorophyll a (Chl*a*), fucoxanthin, carotene, diadinoxanthin and the violaxanthin cycle pigments (VAZ) violaxanthin (V), antheraxanthin (A), and zeaxanthin (Z) were quantified according to Van Heukelem and Thomas (2001).

*Carbon fixation*: Net rates of carbon fixation were measured as $^{14}$C-incorporation over 24 h. This incubation period was chosen because it reliably provides net rates of carbon fixation, while shorter-term incubations can result in estimates somewhere between gross and net rates, depending on species and growth conditions (Milligan et al. 2015). For each of the triplicate cultures two 20 mL aliquots at $5 \times 10^4$ cells $\cdot$ mL$^{-1}$ of *Ochromonas* received 250 μCi $^{14}$C-bicarbonate at the onset of the light period. Depending on the treatment, the cultures contained either $3 \times 10^7$ cells mL$^{-1}$ of *Vibrio fischeri* (prey-amended treatments) or no prey (prey-deplete treatments). One aliquot was incubated with light intensity and diel cycle matching acclimation conditions (15 or 100 μmol photons $\cdot$ m$^{-2}$ $\cdot$ s$^{-1}$) and the second served as dark control. After 24 h incubation, 100 μL samples from $^{14}$C-incubations was added to 10 mL scintillation cocktail (CytoScint; MP Biomedicals, Santa Ana, CA, USA) to measure the total $^{14}$C-activity. The remaining cultures from $^{14}$C-incubations were filtered onto 25-mm GF/F filters to measure activities in samples and dark control, respectively. Filters were incubated in 5% HCl overnight to remove inorganic $^{14}$C. After receiving 10 mL of scintillation, cocktail samples were measured on a scintillation counter (Beckman Coulter LS 6500, Indianapolis, IN, USA). Rates of carbon fixation were calculated according to Pennington and Chavez (2000) and converted to cellular rates of carbon fixation using the mean *Ochromonas* abundance accounting for growth over the incubation time (Heinbokel 1978).

*Ingestion rates*: Ingestion rates were measured by prey disappearance relative to a prey only control. For each strain and light intensity, triplicate cultures were diluted to $5 \times 10^4$ cells mL$^{-1}$ and *Vibrio fischeri* was added to a final abundance of $3 \times 10^7$ cells $\cdot$ mL$^{-1}$. Triplicate control flasks received the same abundance of *V. fischeri* and a volume of culture filtrate (0.2 μm) equal to the culture volume added to the grazing treatment. Flow cytometry samples were taken after 0 and 24 h of incubation and fixed, stored, and counted on the Influx as described above. Ingestion rates were calculated according to Heinbokel (1978). For measurement of prey carbon content, duplicate 20 mL aliquots of *V. fischeri* stock used as bacterial prey were filtered onto pre-combusted GF-75 filters (Advantec, Dublin, CA, USA), stored at −20°C and dried at 50°C overnight prior to analysis at the analytical facility of Horn Point Laboratory at the University of Maryland, Center

for Environmental Science. Live *V. fischeri* used for the experiments had a carbon content of 0.069 ± 0.014 pg C · cell$^{-1}$.

*Fluorescence kinetics of photosystem II (PSII)*: FRRf was used to measure PSII fluorescence kinetics. Rapid light–response curves were recorded using a sequence of eight light intensities from 0 to 300 µmol photons · m$^{-2}$ · s$^{-1}$. Cultures were exposed to the respective light intensity for 3 min before performing four series of measurements at 20 s time intervals. For dark acclimated readings ($F_0$ and $F_m$), cultures were incubated in darkness for 25 min prior to measurements. The excitation and relaxation protocols are described in Guo et al. (2018). During excitation, fluorescence rises from a minimum ($F_0$) or steady-state ($F'_s$) value in dark-acclimated cultures or in actinic light, respectively, to a maximum ($F_m$ or $F'_m$ in darkness or actinic light, respectively) as reaction centers close during light saturation. Fluorescence parameters and the effective absorption cross-section of PSII ($\sigma_{PSII}$ in Å$^2$) were derived according to Kolber et al. (1998). Effective quantum efficiency of PSII was derived as $\Delta F/F'_m=(F'_m - F'_s)/F'_m$ and maximum quantum efficiencies were calculated from dark acclimated readings as $F_v/F_m=(F_m - F_0)/F_m$. Rates of electron transport per functional reaction center of PSII ($ETR_{RCII}$) were estimated as in Schuback et al. (2015):

$$ETR_{RCII} = E \times \sigma_{PSII} \times \left(\frac{\Delta F/F'_m}{F_v/F_m}\right) \times 6.022 \times 10^{-3}$$

where $E$ is irradiance and the factor $6.022 \times 10^{-3}$ converts µmol photons to photons and Å$^2$ to m$^2$. The exponential photosynthesis–irradiance curve (Webb et al. 1974)

$$ETR = ETR_{max}\left(1 - e^{-\frac{\alpha E}{ETR_{max}}}\right)$$

was fitted to $ETR_{RCII}$ data from rapid light–response curves using the iterative least-square nonlinear regression in Sigma-Plot 13. Non-photochemical quenching (NPQ) was calculated as:

$$NPQ = \frac{(F_m - F'_m)}{F'_m}.$$

CCMP1393 exhibited maximum fluorescence values ($F_{max}$) in low light instead of darkness and $F_{max}$ therefore replaced $F_m$ in the calculation of NPQ.

*Inhibition of mitochondrial and chloro-respiration*: The influence of mitochondrial and chloro-respiration on electron transport through PSII was assessed by FRRf measurements in the presence of inhibitors. Plastid terminal oxidase (PTOX), the electron acceptor in chlororespiration, was inhibited by 1 mM propylgallate (Bailey et al. 2008). The mitochondrial alternative oxidase (AOX) and respiratory complex III ($C_{III}$) were inhibited by 1 mM salicylhydroxamic acid and 5 µM antimycin A, respectively (Bailleul et al. 2015). A combination of salicylhydroxamic acid and antimycin A was used to block mitochondrial respiration completely. Readings were taken using prey-amended cultures pre-acclimated to 100 µmol photons · m$^{-2}$ · s$^{-1}$ and subjected to 3 min of illumination by 20, 100, and 300 µmol photons · m$^{-2}$ · s$^{-1}$ prior to the measurement representative of sub-saturating, near-saturating, and super-saturating light intensities relative to acclimation conditions. The effect of mitochondrial inhibitors on photosynthetic electron transport is expressed as relative decrease in the effective quantum efficiency of PSII ($\Delta F/F'_m$) compared to the control reading acquired before addition of inhibitors.

*Statistics*: To detect differences in growth between autotrophic, mixotrophic, and heterotrophic conditions over time growth curves were analyzed by repeated measures ANOVA. Pigment contents and carbon fixation were tested for differences between isolates as well as effects of light intensity and prey availability by three-way ANOVA. Effects of light and prey availability were also analyzed separately for each isolate by two-way ANOVA to assess their impact and interaction in each isolate individually. Because ingestion rates can only be measured in prey-amended treatments, a two-way ANOVA was used for the full data set, while a one-way ANOVA tested for the effect of light in each isolate individually. Carotene to Chl*a* ratios were log-transformed to improve homoscedasticity. FRRf measurements of rapid light–response curves and inhibitor tests were analyzed by repeated measures ANOVA with light as repeated factor. Holm-Sidak tests were performed for all post-hoc pairwise comparisons.

## RESULTS

*Phylogenetic tree of chrysophytes.* The distribution of nutritional strategies across the phylogenetic tree of chrysophytes is complex, based on the current level of understanding and available isolates (Fig. 1). The orders Hibberdiales and Synurales are composed of presumably purely photosynthetic organisms, while Paraphysomonadida and Apoikiida contain solely non-photosynthetic organisms. The two isolates studied here have 97% nucleotide identity between their 18S rRNA genes and belong to the Ochromonadales, a group which contains both mixotrophic and purely heterotrophic taxa. Moreover, the presence of heterotrophic taxa in several Ochromonadales subclades suggests photosynthetic machinery has been lost multiple times within this group.

*Light–response curves (Experiment 1).* The two isolates of *Ochromonas* showed pronounced differences in their responses to resource availability. When both light and prey were available to support mixotrophic nutrition CCMP1393 and CCMP2951 reached maximum growth rates of 0.58 ± 0.04 and 0.82 ± 0.04 · d$^{-1}$, respectively (Fig. 2, a and b). Under these conditions, differences in responses to light intensity were reflected in adjustments of cellular red fluorescence levels. CCMP1393 showed increased red fluorescence at low-light intensities (Fig. 2a; ANOVA: $F_{4,10} = 196.8$, $P < 0.001$), while CCMP2951 showed decreased fluorescence when shifting to a more

FIG. 1. Phylogenetic reconstruction of chrysophytes based on 18S rRNA gene sequences. A total of 1,444 positions from 132 near full-length sequences were used. Tree topology is based on maximum likelihood inference and node statistical supports are indicated based on Bayesian posterior node probabilities, and percent of bootstrap replicates from two maximum likelihood methods (1,000 replicates in RAxML and 100 replicates in PhyML). Columns of colored squares indicate the nutritional capacities of described genera for photosynthesis (left column: green—known phototrophic potential, white—potential not reported in cultured isolates, grey—unknown potential) and for phagotrophic ingestion of prey (right column: black—known phagotrophic potential, white—potential not reported in cultured isolates, grey—unknown potential). [Color figure can be viewed at wileyonlinelibrary.com]

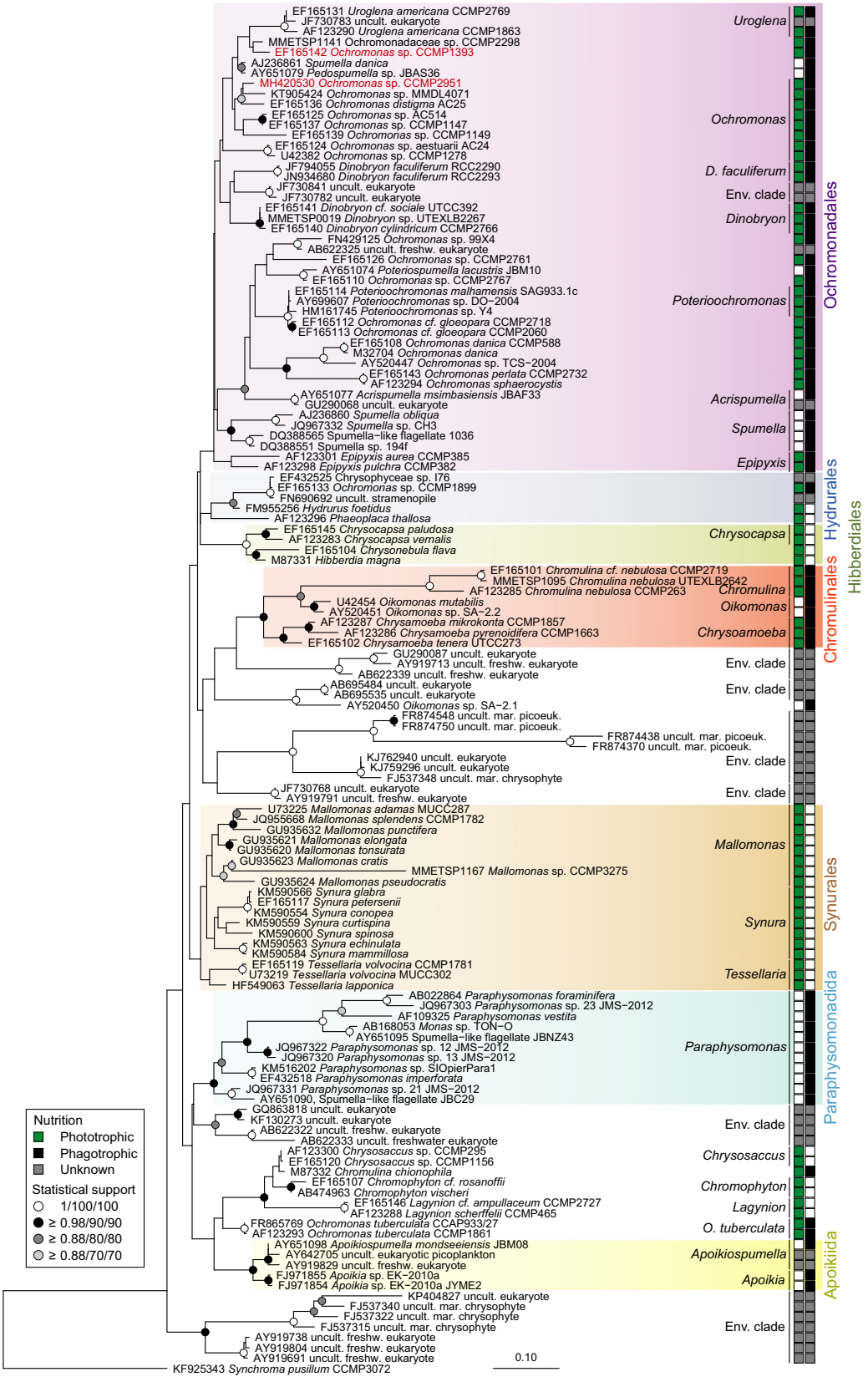
EF165131 Uroglena americana CCMP2769
JF730783 uncult. eukaryote
AF123290 Uroglena americana CCMP1863
MMETSP1141 Ochromonadaceae sp. CCMP2298
EF165142 Ochromonas sp. CCMP1393
AJ236861 Spumella danica
AY651079 Pedospumella sp. JBAS36
MH420530 Ochromonas sp. CCMP2951
KT905424 Ochromonas sp. MMDL4071
EF165136 Ochromonas distigma AC25
EF165125 Ochromonas sp. AC514
EF165137 Ochromonas sp. CCMP1147
EF165139 Ochromonas sp. CCMP1149
EF165124 Ochromonas sp. aestuarii AC24
U42382 Ochromonas sp. CCMP1278
JF794055 Dinobryon faculiferum RCC2290
JN934680 Dinobryon faculiferum RCC2293
JF730841 uncult. eukaryote
JF730782 uncult. eukaryote
EF165141 Dinobryon cf. sociale UTCC392
MMETSP0019 Dinobryon sp. UTEXLB2267
EF165140 Dinobryon cylindricum CCMP2766
FN429125 Ochromonas sp. 99X4
AB622325 uncult. freshw. eukaryote
EF165126 Ochromonas sp. CCMP2761
AY651074 Poteriospumella lacustris JBM10
EF165110 Ochromonas sp. CCMP2767
EF165114 Poterioochromonas malhamensis SAG933.1c
AY699607 Poterioochromonas sp. DO−2004
HM161745 Poterioochromonas sp. Y4
EF165112 Ochromonas cf. gloeopara CCMP2718
EF165113 Ochromonas cf. gloeopara CCMP2060
EF165108 Ochromonas danica CCMP588
M32704 Ochromonas danica
AY520447 Ochromonas sp. TCS−2004
EF165143 Ochromonas perlata CCMP2732
AF123294 Ochromonas sphaerocystis
AY651077 Acrispumella msimbasiensis JBAF33
GU290068 uncult. eukaryote
AJ236860 Spumella obliqua
JQ967332 Spumella sp. CH3
DQ388565 Spumella−like flagellate 1036
DQ388551 Spumella sp. 194f
AF123301 Epipyxis aurea CCMP385
AF123298 Epipyxis pulchra CCMP382
EF432525 Chrysophyceae sp. I76
EF165133 Ochromonas sp. CCMP1899
FN690692 uncult. stramenopile
FM955256 Hydrurus foetidus
AF123296 Phaeoplaca thallosa
EF165145 Chrysocapsa paludosa
AF123283 Chrysocapsa vernalis
EF165104 Chrysonebula flava
M87331 Hibberdia magna
EF165101 Chromulina cf. nebulosa CCMP2719
MMETSP1095 Chromulina nebulosa UTEXLB2642
AF123285 Chromulina nebulosa CCMP263
U42454 Oikomonas mutabilis
AY520451 Oikomonas sp. SA−2.2
AF123287 Chrysamoeba mikrokonta CCMP1857
AF123286 Chrysamoeba pyrenoidifera CCMP1663
EF165102 Chrysamoeba tenera UTCC273
GU290087 uncult. eukaryote
AY919713 uncult. freshw. eukaryote
AB622339 uncult. freshw. eukaryote
AB695484 uncult. eukaryote
AB695535 uncult. eukaryote
AY520450 Oikomonas sp. SA−2.1
FR874548 uncult. mar. picoeuk.
FR874750 uncult. mar. picoeuk.
FR874438 uncult. mar. picoeuk.
FR874370 uncult. mar. picoeuk.
KJ762940 uncult. eukaryote
KJ759296 uncult. eukaryote
FJ537348 uncult. mar. chrysophyte
JF730768 uncult. eukaryote
AY919791 uncult. freshw. eukaryote
U73225 Mallomonas adamas MUCC287
JQ955668 Mallomonas splendens CCMP1782
GU935632 Mallomonas punctifera
GU935621 Mallomonas elongata
GU935620 Mallomonas tonsurata
GU935623 Mallomonas cratis
MMETSP1167 Mallomonas sp. CCMP3275
GU935624 Mallomonas pseudocratis
KM590566 Synura glabra
EF165117 Synura petersenii
KM590554 Synura conopea
KM590559 Synura curtispina
KM590600 Synura spinosa
KM590563 Synura echinulata
KM590584 Synura mammillosa
EF165119 Tessellaria volvocina CCMP1781
U73219 Tessellaria volvocina MUCC302
HF549063 Tessellaria lapponica
AB022864 Paraphysomonas foraminifera
JQ967303 Paraphysomonas sp. 23 JMS−2012
AF109325 Paraphysomonas vestita
AB168053 Monas sp. TON−O
AY651095 Spumella−like flagellate JBNZ43
JQ967322 Paraphysomonas sp. 12 JMS−2012
JQ967320 Paraphysomonas sp. 13 JMS−2012
KM516202 Paraphysomonas sp. SIOpierPara1
EF432518 Paraphysomonas imperforata
JQ967331 Paraphysomonas sp. 21 JMS−2012
AY651090, Spumella−like flagellate JBC29
GQ863818 uncult. eukaryote
KF130273 uncult. eukaryote
AB622322 uncult. freshw. eukaryote
AB622333 uncult. freshwater eukaryote
AF123300 Chrysosaccus sp. CCMP295
EF165120 Chrysosaccus sp. CCMP1156
M87332 Chromulina chionophila
EF165107 Chromophyton cf. rosanoffii
AB474963 Chromophyton vischeri
EF165146 Lagynion cf. ampullaceum CCMP2727
AF123288 Lagynion scherffelii CCMP465
FR865769 Ochromonas tuberculata CCAP933/27
AF123293 Ochromonas tuberculata CCMP1861
AY651098 Apoikiospumella mondseeiensis JBM08
AY642705 uncult. eukaryotic picoplankton
AY919829 uncult. freshw. eukaryote
FJ971855 Apoikia sp. EK−2010a
FJ971854 Apoikia sp. EK−2010a JYME2
KP404827 uncult. eukaryote
FJ537340 uncult. mar. chrysophyte
FJ537322 uncult. mar. chrysophyte
FJ537315 uncult. mar. chrysophyte
AY919738 uncult. freshw. eukaryote
AY919804 uncult. freshw. eukaryote
AY919691 uncult. freshw. eukaryote
KF925343 Synchroma pusillum CCMP3072
0.10
Uroglena
Ochromonas
D. faculiferum
Env. clade
Dinobryon
Poterioochromonas
Acrispumella
Spumella
Epipyxis
Chrysocapsa
Chromulina
Oikomonas
Chrysoamoeba
Env. clade
Env. clade
Env. clade
Env. clade
Mallomonas
Synura
Tessellaria
Paraphysomonas
Env. clade
Chrysosaccus
Chromophyton
Lagynion
O. tuberculata
Apoikiospumella
Apoikia
Env. clade
Ochromonadales
Hydrurales
Hibberdiales
Chromulinales
Synurales
Paraphysomonadida
Apoikiida
Nutrition
Phototrophic
Phagotrophic
Unknown
Statistical support
1/100/100
≥ 0.98/90/90
≥ 0.88/80/80
≥ 0.88/70/70

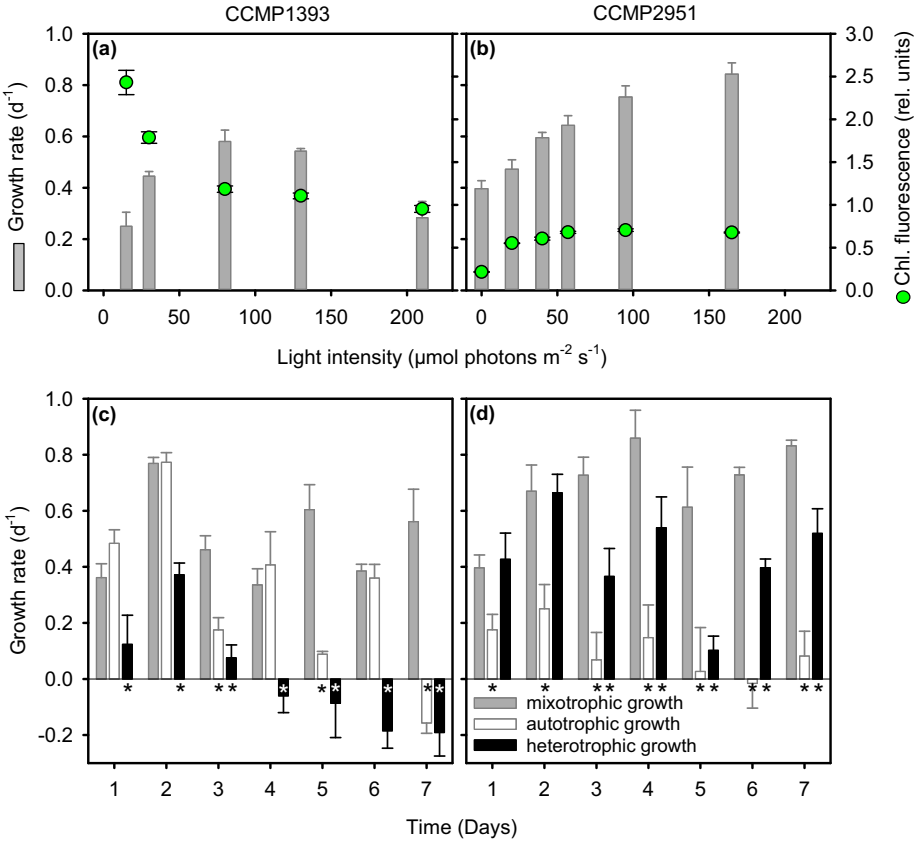


FIG. 2. Growth responses to light under prey-amended conditions in the two *Ochromonas* isolates. (a and b) Light–response curves and cellular chlorophyll *a* fluorescence of CCMP1393 and CCMP2951 during prey-amended growth in the light (mixotrophic growth; Experiment 1). Cultures were maintained semi-continuously with daily additions of *Vibrio fischeri* as prey. (c and d) Growth curves of CCMP1393 and CCMP2951 (Experiment 2) with daily prey-amendments in the light (mixotrophic growth), with daily prey-amendments in darkness (heterotrophic growth), or after ceasing prey-amendments in the light (autotrophic growth). Asterisk indicates significant difference from mixotrophic conditions ($P < 0.05$; Holm-Sidak test following a two-way repeated measures ANOVA). Error bars indicate standard deviation among biological triplicates. [Color figure can be viewed at wileyonlinelibrary.com]

heterotrophic nutrition at low-light intensities (Fig. 2b; ANOVA: $F_{5,12} = 825.7$, $P < 0.001$). CCMP1393 exhibited photoinhibition at 210 µmol photons $\cdot$ m$^{-2}$ $\cdot$ s$^{-1}$, while CCMP2951 did not show signs of photoinhibition over the range of light levels tested (maximum 180 µmol photons m$^{-2}$ s$^{-1}$).

*Autotrophic and heterotrophic growth potential (Experiment 2).* When kept in darkness, CCMP1393 started to die after 3 d (Fig. 2c), while CCMP2951 could maintain growth rates of $0.40 \pm 0.03 \cdot d^{-1}$ by heterotrophy with bacterial prey as the only source of carbon. After daily prey-amendments had ceased, CCMP1393 maintained relatively high growth rates for a few days after depleting prey, whereas CCMP2951 showed an immediate drop in growth rates (Fig. 2, c and d). However, after 7 d without feeding CCMP1393 began to die while CCMP2951 did not exhibit measureable death rates.

*Response to light limitation and depletion of prey (Experiment 3).* In line with these different resource requirements, the two isolates responded differently to light limitation and the depletion of prey over a period of 3 d. Time courses of prey depletion were similar among isolates, although CCMP2951 depleted its prey less strongly at low-light intensities (Figure S1 in the Supporting Information). In CCMP1393, photosynthetic carbon fixation was nearly halved after prey had been depleted in the high-light treatment, while it remained unchanged in CCMP2951 (Fig. 3a; two-way ANOVA, Table 1). For both isolates, the 7-fold decrease in light intensity, from near-optimal to limiting conditions, significantly reduced net rates of carbon fixation (Fig. 3a; three-way ANOVA, effect of light, Table 1), although their responses differed significantly (three-way ANOVA, light × isolate interaction, Table 1). While rates of carbon fixation decreased 12- to 20-fold in CCMP2951, they only decreased 4- to 6-fold in CCMP1393 (Fig. 3a). This difference is in line with the increased chlorophyll content of CCMP1393 at low-light intensities (Fig. 4a; two-way ANOVA, Table 1). Ingestion rates showed a different pattern to cellular chlorophyll content with a significant increase at higher light intensity in CCMP1393 and decrease in CCMP2951 (Fig. 3b; two-way ANOVAs, Table 1). Hence, in prey-

amended cultures carbon fixation and ingestion covaried in response to light intensity in CCMP1393, while they were inversely related in CCMP2951. Although low prey and light availabilities both led to reduced growth in both isolates (Fig. 3c; $P < 0.001$, Table 1), their responses to these resources differed significantly (two-way ANOVA interaction terms, Table 1). CCMP1393 grew generally faster in high-light conditions, while CCMP2951 always showed higher growth rates when prey-amended. Overall, the larger dependency on photosynthesis in CCMP1393 resulted in a relatively stronger reduction of growth under low-light conditions (67%) compared to CCMP2951 (37%). Under low-light carbon fixation was not sufficient for survival of CCMP1393 after prey depletion resulting in a population decrease, while at light-saturation the decrease in growth after prey depletion (55%) was less severe than in CCMP2951 (72%). Note that ingestion rates represent gross carbon uptake from prey, while carbon fixation is represented by net rates. Therefore, measured rates of carbon acquisition cannot be directly linked to growth responses. A decrease in FALS upon prey depletion (Figure S2 in the Supporting Information) indicates decreased cell sizes, which might further skew the relationship between cellular carbon acquisition and specific growth rates.

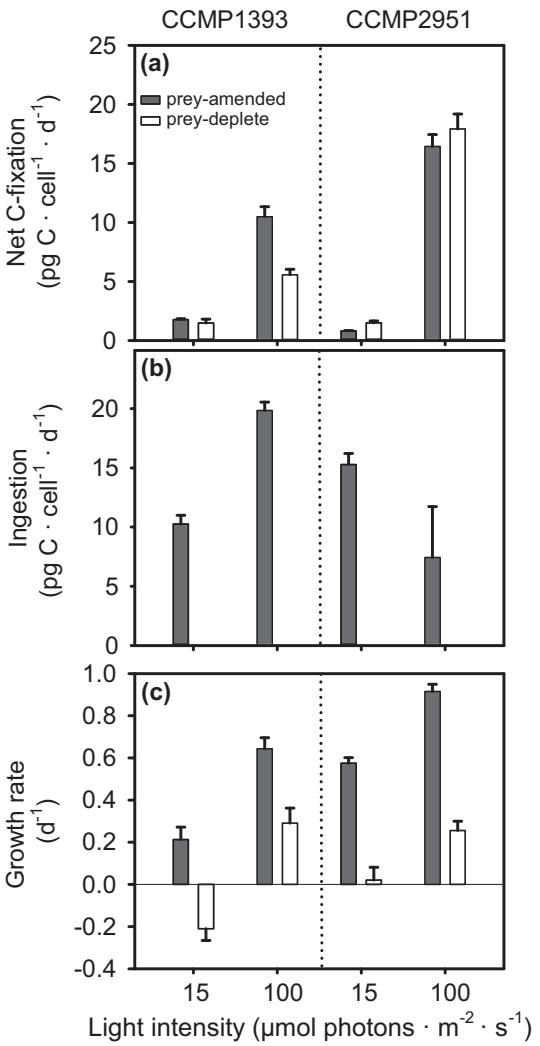


FIG. 3. Carbon acquisition and growth of the two *Ochromonas* isolates under prey-amended and deplete conditions. Rates of (a) net primary production, (b) ingestion, and (c) growth in CCMP1393 and CCMP2951 acclimated to 15 (LL) or 100 (HL) µmol photons · $m^{-2}$ · $s^{-1}$ under either prey-amended or prey-deplete conditions. Error bars indicate standard deviation among biological triplicates. For figure simplicity, results of statistical comparisons are shown in Table 1.

Changes in pigmentation in response to light and prey availability also differed between isolates (Fig. 4; ANOVA interaction terms, Table 1). Cellular Chl*a* content increased significantly under low-light compared to high-light conditions in CCMP1393, but not in CCMP2951 (Fig. 4a; two-way ANOVAs, Table 1), as already indicated by red fluorescence. Prey depletion was associated with decreases in cellular chlorophyll content in CCMP1393, but there was no significant change in CCMP2951 (Table 1). This pattern is in line with the stronger reduction in FALS and therefore possibly cell size observed in CCMP1393 upon prey depletion (Fig. S2). The adjustment of accessory pigments relative to Chl*a* was more comparable between isolates with fucoxanthin being slightly increased at low-light intensities (three-way ANOVA, Table 1). The photo-protective pigment carotene was present at higher concentrations in CCMP2951 and increased at high-light intensities in both isolates (three-way ANOVA, Table 1). The same was true for diadinoxanthin which was present at 13-fold higher concentrations in CCMP2951 compared to CCMP1393 under prey-amended conditions when acclimated to near-optimal high-light intensity (Figure S3 in the Supporting Information). In low-light acclimated CCMP1393, diadinoxanthin was not detectable. The de-epoxidized form diatoxanthin, that is part of the diadinoxanthin cycle in diatoms (Arsalane et al. 1994), was not detected in either *Ochromonas* isolate. The ratio of violaxanthin cycle pigments (VAZ-pigments) to Chl *a* was comparable among isolates and elevated under high-light acclimation (Fig. 4d; three-way ANOVA, Table 1). In CCMP2951, it was significantly higher during prey-amended compared to prey-deplete conditions, while the opposite trend was observed in CCMP1393 (two-way ANOVA, Table 1).

Maximum $ETR_{RCII}$ ($ETR_{max}$) was reduced in low-light compared to near-optimal, high-light acclimated cultures (Fig. 5, a and b, Table 2) and this effect was strongest in CCMP2951. $ETR_{RCII}$ did not show photoinhibition in response to short-term exposure to super-saturating light intensities, even though photoinhibition had been observed in acclimated growth rates of CCMP1393 (Fig. 2a). The capacity for non-photochemical quenching (NPQ)

TABLE 1. Statistical analysis of results from Experiment 3. Effects of *Ochromonas* isolate phylogenetic identity, light intensity, and prey availability as well as their interactions in a three-way ANOVA and effects of light intensity, and prey availability as well as their interaction in each isolate individually by a two-way ANOVA. Shown are effects on carbon fixation (Cfix), rates of ingestion and growth, as well as Chl*a* content, and relative contents of carotene (Caro), fucoxanthin (Fuco), and violaxanthin cycle pigments (VAZ). Arrows indicate the direction of significant responses with increasing light intensity or prey availability, respectively.

| | | | | Three-way ANOVA | | | | Two-way ANOVA | |
|---|---|---|---|---|---|---|---|---|---|
| | | | | Single effect | | Isolate Interaction | | | |
| Parameter | Factor | df1 | df2 | *F* | *P* | *F* | *P* | CCMP1393 | CCMP2951 |
| Cfix/ cell | Isolate | 1 | 16 | 26.6 | <0.001 | | | | |
| Cfix/ cell | Light | 1 | 16 | 2668 | <0.001 | 204.2 | <0.001 | ↑[a] | ↑[a] |
| Cfix/ cell | Prey | 1 | 16 | 0.64 | 0.436 | 83.0 | <0.001 | ↑[a] | -[a] |
| Ingestion | Isolate | 1 | 8 | 8.01 | 0.022 | | | | |
| Ingestion | Light | 1 | 8 | 0.44 | 0.526 | 44.8 | <0.001 | ↑ | ↓[a] |
| Growth | Isolate | 1 | 16 | 93.9 | <0.001 | | | | |
| Growth | Light | 1 | 16 | 309.9 | <0.001 | 17.2 | 0.001 | ↑[a] | ↑[a] |
| Growth | Prey | 1 | 16 | 540.3 | <0.001 | 26.2 | <0.001 | ↑[a] | ↑[a] |
| Chl *a*/cell | Isolate | 1 | 16 | 1.58 | 0.227 | | | | |
| Chl *a*/cell | Light | 1 | 16 | 6.01 | 0.025 | 34.6 | <0.001 | ↓[a] | -[a] |
| Chl *a*/cell | Prey | 1 | 16 | 17.3 | <0.001 | 36.5 | <0.001 | ↑[a] | -[a] |
| Caro/Chl *a* | Isolate | 1 | 16 | 6810 | <0.001 | | | | |
| Caro/Chl *a* | Light | 1 | 16 | 2742 | <0.001 | 427 | <0.001 | ↑[a] | ↑[a] |
| Caro/Chl *a* | Prey | 1 | 16 | 30.2 | <0.001 | 0.70 | 0.416 | ↓[a] | ↓[a] |
| Fuco/Chl *a* | Isolate | 1 | 16 | 363 | <0.001 | | | | |
| Fuco/Chl *a* | Light | 1 | 16 | 157 | <0.001 | 1.58 | 0.226 | ↓ | ↓[a] |
| Fuco/Chl *a* | Prey | 1 | 16 | 5.81 | 0.028 | 8.94 | 0.009 | ↓ | -[a] |
| VAZ/Chl *a* | Isolate | 1 | 16 | 963 | <0.001 | | | | |
| VAZ/Chl *a* | Light | 1 | 16 | 2205 | <0.001 | 96.2 | <0.001 | ↑[a] | ↑ |
| VAZ/Chl *a* | Prey | 1 | 16 | 0.03 | 0.865 | 82.7 | <0.001 | ↓[a] | ↑ |

[a]Significant interaction of prey and light availability ($P < 0.05$).

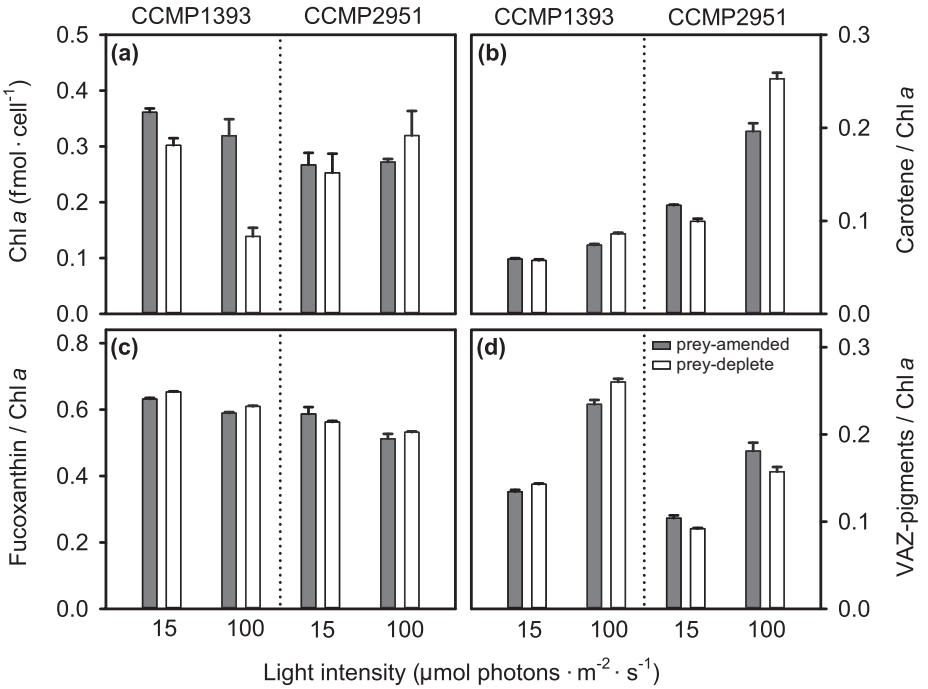


FIG. 4. Pigmentation of the two *Ochromonas* isolates under prey-amended and prey-deplete conditions. (a) Cellular chlorophyll content and relative content of (b) carotene, (c) fucoxanthin, and (c) Violaxanthin cycle pigments (VAZ) in CCMP1393 and CCMP2951 acclimated to 15 (LL) or 100 (HL) µmol photons · $m^{-2}$ · $s^{-1}$ under either prey-amended or prey-deplete conditions. Relative pigment contents are expressed as molar ratios to Chl *a*. Error bars indicate standard deviation among biological triplicates. For figure simplicity, results of statistical comparisons are shown in Table 1.

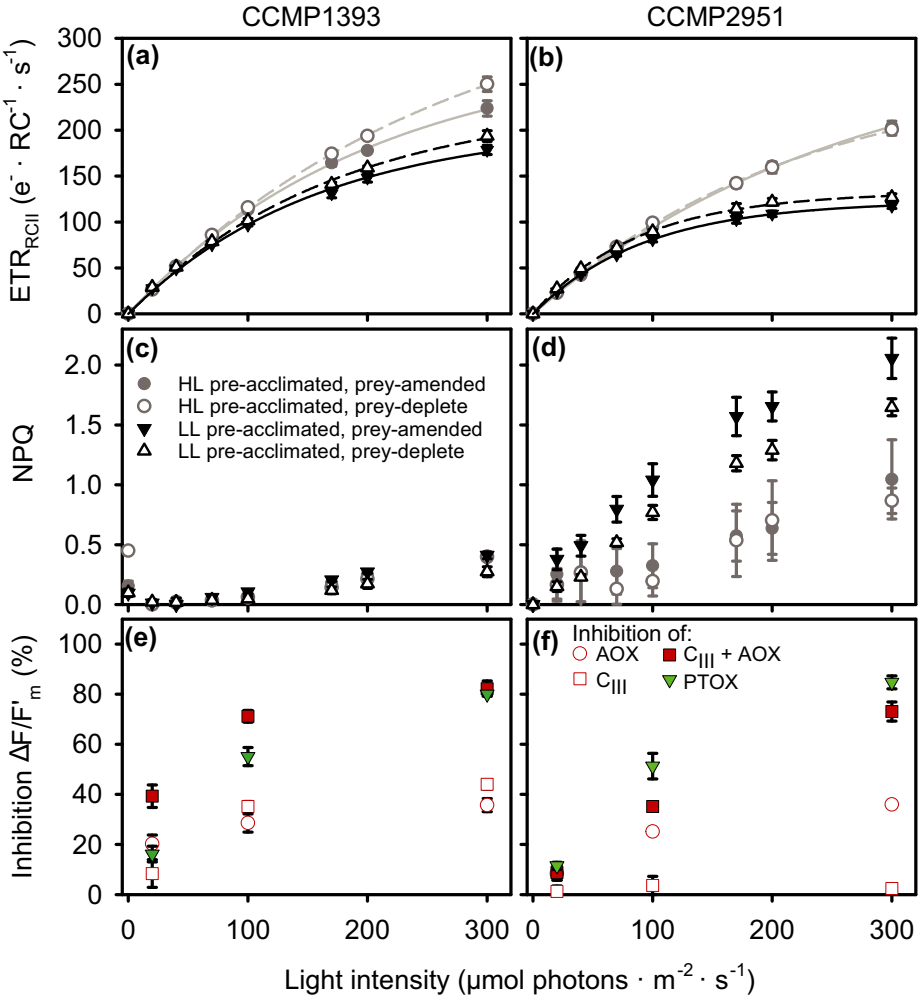


FIG. 5. Electron transport in the two *Ochromonas* isolates under prey-amended and deplete conditions. (a and b) Rapid light–response curves of electron transport through photosystem II. Lines represent photosynthesis–irradiance curves fitted to the data (see Table 2 for parameter values). (c and d) Non-photochemical quenching (NPQ) in CCMP1393 and CCMP2951 pre-acclimated to low-light (15 µmol photons · $m^{-2}$ · $s^{-1}$) and high-light (100 µmol photons · $m^{-2}$ · $s^{-1}$) intensities under either prey-amended conditions or after depletion of prey for 3 d. (e and f) Effect of inhibition of mitochondrial respiratory complex III ($C_{III}$), mitochondrial alternative oxidase (AOX), both $C_{III}$ and AOX, or the plastid terminal oxidase (PTOX) involved in chlororespiration on effective photochemical yield of PSII in CCMP1393 and CCMP2951. Measurements were performed with mixotrophic, prey-amended cultures acclimated to 100 µmol photons · $m^{-2}$ · $s^{-1}$ and exposed to a sub-saturating light intensity, the acclimation intensity, or a super-saturating intensity for a period of 3 min prior to measurements. Error bars indicate standard deviation among biological triplicates. [Color figure can be viewed at wileyonlinelibrary.com]

differed largely between isolates (Fig 5 c and d). CCMP1393 exhibited only modest levels of NPQ, while CCMP2951 showed strong NPQ upon exposure to high-light intensities, especially in the cultures that had been pre-acclimated to low-light intensities. Additionally, for low-light acclimated CCMP2951, the NPQ response was stronger in prey-amended compared to prey-deplete cultures (Holm-Sidak test, $P < 0.02$ for actinic light >100 µmol photons · $m^{-2}$ · $s^{-1}$).

To assess alternative routes of electron transport and their role in photosynthesis, three specific inhibitors were used, targeting PTOX involved in chlororespiration or the mitochondrial electron acceptors $C_{III}$ and AOX, respectively. In both isolates, inhibition of mitochondrial- or chloro-respiration increasingly modified the effective quantum yield of PSII under exposure to increasing light intensities (Fig. 5, e and f; RM-ANOVA: $F_{2,1} = 697$, $P < 0.001$ for CCMP1393 and $F_{2,1} = 491$, $P < 0.001$ for CCMP2951). This indicates both pathways act as an overflow mechanism for reducing equivalents produced by the photosynthetic machinery. In CCMP1393, photosynthetic yield was affected by inhibition of $C_{III}$ and AOX both individually and in combination. Inhibition of the entire mitochondrial respiration already affected photosynthetic electron transport at sub-saturating light intensities (Holm-Sidak test, $P < 0.001$ for combination of inhibitors compared to each individual one at 20 µmol photons · $m^{-2}$ · $s^{-1}$) and this effect did not increase strongly moving into saturating and super-saturating intensities (100 and 300 µmol photons ·

TABLE 2. Parameters of photosynthesis-irradiance curve fits to rapid light–response curves of the two *Ochromonas* isolates based on electron transport rates (Fig. 5, a and b). Light intensities are given in μmol photons · $m^{-2}$ · $s^{-1}$. Values in parentheses give estimates of standard errors.

| Isolate | Light | Prey | $ETR_{max}$ | α | adj $r^2$ |
|---|---|---|---|---|---|
| CCMP1393 | 100 | amended | 289 (±8) | 1.42 (±0.07) | 0.998 |
| CCMP1393 | 100 | deplete | 370 (±10) | 1.37 (±0.05) | 0.999 |
| CCMP1393 | 15 | amended | 207 (±5) | 1.30 (±0.07) | 0.996 |
| CCMP1393 | 15 | deplete | 232 (±5) | 1.35 (±0.05) | 0.997 |
| CCMP2951 | 100 | amended | 303 (±8) | 1.12 (±0.04) | 0.999 |
| CCMP2951 | 100 | deplete | 271 (±8) | 1.19 (±0.06) | 0.998 |
| CCMP2951 | 15 | amended | 123 (±1) | 1.33 (±0.04) | 0.997 |
| CCMP2951 | 15 | deplete | 133 (±2) | 1.52 (±0.06) | 0.996 |

$m^{-2} \cdot s^{-1}$, respectively). In CCMP2951, photosynthesis was affected by inhibition of AOX but not by inhibition of $C_{III}$. The simultaneous inhibition of both mitochondrial electron acceptors had no significant effect at sub-saturating light intensities, but caused a stronger effect compared to inhibition of AOX alone, at higher light intensities (Holm-Sidak test, $P < 0.001$ for combination of inhibitors compared to each individual one at 100 and 300 μmol photons · $m^{-2} \cdot s^{-1}$).

## DISCUSSION

The two mixotrophic chrysophytes studied here showed opposite physiological responses to environmental drivers. The capability of CCMP2951 to adjust its nutrition from pure heterotrophy in darkness to mixotrophy in the light and at least survival by autotrophy in the absence of prey characterizes it as a facultative mixotroph, albeit tending more toward the heterotrophic side of the mixotrophic spectrum. Overall, the phenotypic plasticity in its nutrition should facilitate growth under a wide range of environmental conditions. Similar to CCMP2951, CCMP1393 shows very poor autotrophic growth in the absence of prey, although it is able to maintain growth for a few days without feeding (Fig. 2). It might thus have a slightly lower requirement for prey and tend more toward the autotrophic side of the mixotrophic spectrum compared to CCMP2951. CCMP1393 is furthermore unable to grow heterotrophically in darkness, and hence is an obligate mixotroph that requires both light and prey for growth, at least under the conditions tested herein. These different physiologies appear to be rooted in the interaction between photosynthetic and heterotrophic processes, resulting in distinct ecological strategies for these two chrysophytes. The two isolates thus likely represent different species, as also supported by morphological differences with an eyespot present in only CCMP2951 and detectable differences in their 18S rRNA genes. While their 97% nucleotide identity in 18S rRNA genes indicates close relatedness, this gene is strongly conserved and does not always provide sufficient resolution to distinguish closely related species. The percentage of shared genes in their genomes might, for instance, be much lower as reported in two green algal *Micromonas* species (Worden et al. 2009). Overall, our results exemplify the difficulties in linking phylogenetic to functional diversity of mixotrophs (Figs. 1 and 6).

Organisms with a mixotrophic lifestyle face a trade-off between investments into nutrient uptake, photosynthesis, and phagotrophy (Andersen et al. 2015). Modeling studies suggest that differential investment into optimization of these traits underlies successional patterns of phytoplankton (Berge et al. 2017). Similarly, the high phenotypic plasticity in the facultative mixotroph CCMP2951 observed here reflects differential investment into these traits that is shaped by environmental conditions. At low-light intensities, increased ingestion rates substitute for photosynthesis and make additional investment into chlorophyll biosynthesis obsolete. The capacity of phagotrophy to sustain growth in darkness is in agreement with previous studies of predominantly heterotrophic freshwater isolates of *Ochromonas* and *Poterioochromonas* (Andersson et al. 1989, Sanders et al. 1990, Wilken et al. 2013), although its maximum growth and ingestion rates observed here are lower than reported for freshwater *Ochromonas* isolates (Rothhaupt 1996, Wilken et al. 2013). Moreover, the high nutritional plasticity requires that the two nutritional pathways can principally function independently from each other, as both can supply sufficient resources to fuel cellular metabolism. In particular, under mixotrophic growth at low-light compared to high-light intensities, higher rates of ingestion seem to compensate for the decreased rates of carbon fixation resulting in an inverse relationship between these two rates (Fig. 3). Thus, our results demonstrate that photosynthesis and heterotrophy act as partly substitutable routes of resource acquisition in the facultative mixotroph.

Unlike facultative mixotrophy, photosynthesis and heterotrophy covary in the obligate mixotroph CCMP1393 (Fig. 3) and thus constitute complimentary routes of resource acquisition that cannot function independently from each other. Such a strategy cannot be explained solely by differential investment into resource acquisition traits. Instead, the reliance on the simultaneous performance of both

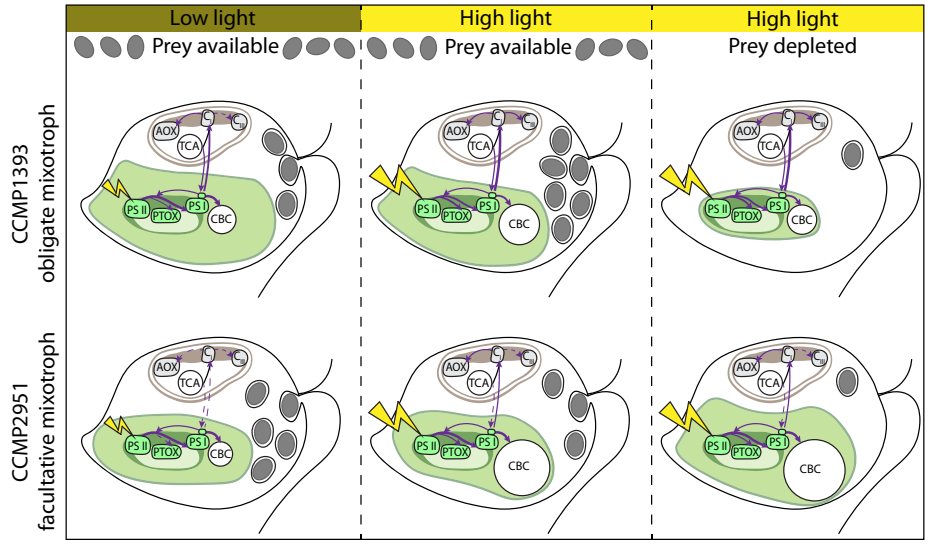


FIG. 6. Responses of the two mixotrophic *Ochromonas* isolates to different environmental conditions. Both isolates reach highest growth rates under saturating light and prey availability. The obligate mixotroph (CCMP1393, top row) has higher chlorophyll content under low-light compared to high-light conditions and when prey is available compared to prey-deplete conditions. Rates of both carbon fixation in the Calvin–Benson cycle (CBC) and ingestion of prey are highest under mixotrophic conditions under high light. Reducing equivalents are exchanged between the plastid and mitochondria linking the photosynthetic with the respirational electron transport chain. Growth is most strongly reduced at low-light intensities. In contrast, the facultative mixotroph (CCMP2951, bottom row) increases its chlorophyll content when prey is depleted at high light, while in the presence of prey light has little impact on chlorophyll content. Rates of ingestion are highest under low-light condition and maximum rates of carbon fixation are reached when prey is depleted. Export of reducing equivalents from the chloroplast to mitochondria only acts as overflow during high-light condition. Growth is most strongly reduced in the absence of prey. AOX, alternative oxidase; TCA, tricarboxylic acid cycle; $C_I$, respiratory complex I; $C_{III}$, respiratory complex III; PSII, photosystem II; PTOX, plastid terminal oxidase; PSI, photosystem I; CBC, Calvin–Benson cycle. [Color figure can be viewed at wileyonlinelibrary.com]

photosynthesis and phagotrophy to attain positive growth rates suggests an integration of these two nutritional pathways that restrict their independent execution. This interdependence of photosynthesis and heterotrophy results in decreased ingestion rates under light limitation and decreased chlorophyll content when prey are lacking, in line with changes in transcriptional patterns observed in this isolate (Lie et al. 2018). Dependency on light for survival has been described in other mixotrophs such as the brackish chrysophyte *Ochromonas minima* (Flöder et al. 2006) and several dinoflagellates (Jeong et al. 2010, Hansen 2011). The increased chlorophyll content in CCMP1393 under low-light conditions (Figs. 2a and 4a) reflects a photoacclimation response typical for photoautotrophs that results in greater light-harvesting capacity under low light to help maintain photosynthesis (MacIntyre et al. 2002). Despite the potential for photosynthetic carbon acquisition, this route is not sufficient to support stable positive growth rates in CCMP1393 under the conditions tested herein (Fig. 2c). A dependence on phagotrophy is usually explained as reflecting a mechanism for acquiring essential growth factors or nutrients from prey. For example, increasing rates of phagotrophy have been observed with increasing light intensity in the freshwater chrysophyte *Dinobryon cylindricum*, and attributed to providing necessary nutrients via prey cell digestion (Caron et al. 1993). Similar dependencies were reported in the chrysophyte *Uroglena americana*, which appears to be more closely related to CCMP1393 than CCMP2951, although support in this region of the tree is largely lacking (Fig. 1), and the dependency was further characterized as being a requirement for bacterially produced phospholipids (Kimura and Ishida 1989). A recent study on CCMP1393 did not detect transcripts that encode nitrate transporters, and concluded that this chrysophyte does not have the capacity to utilize nitrate (Lie et al. 2018). Additionally, based on growth experiments the freshwater chrysophyte *Ochromonas globosa* relies on reduced nitrogen sources (Wilken et al. 2014b). However, in our experiments, both ammonium and nitrate were provided which would presumably obviate reliance on prey as nitrogen source depending on ammonium depletion rates, which can be rapid in algal culture experiments (McDonald et al. 2010). In general, biosynthetic pathways required for purely photoautotrophic growth could have been lost by some constitutive, obligate mixotrophs, although in the absence of complete genome sequences the prevalence of such pathway reductions remains an open question.

An obligate requirement for phagotrophy in photosynthetic eukaryotes can be expected to result in a finely tuned integration of photosynthetic and heterotrophic metabolisms, regardless of whether this is the cause or consequence of an obligately

mixotrophic lifestyle. A close energetic coupling between plastids and mitochondria involving an overflow mechanism for excess reducing equivalents, as well as support of carbon fixation by mitochondrially derived ATP, also occurs in diatoms (Allen et al. 2008, Bailleul et al. 2015). Effects of mitochondrial inhibitors must generally be interpreted with care, as indirect effects are difficult to exclude. Nevertheless, in CCMP1393, photosynthetic electron transport seems to be strongly influenced by mitochondrial respiration (Fig. 6). In addition to its role as an overflow mechanism for reducing equivalents observed in both isolates, mitochondrial respiration acts as an electron sink even under subsaturating light conditions in CCMP1393. It therefore likely represents an integral part of photosynthetic electron flow in this obligate mixotroph, involving both AOX and $C_{III}$, which might be used for ATP production from photosynthetically derived electrons. While this could potentially reduce the need for heterotrophic respiration and hence increase carbon assimilation efficiencies from prey, higher rates of carbon fixation in the presence of prey do not indicate a tendency toward photoheterotrophy as suggested for the freshwater chrysophyte *Ochromonas danica* (Wilken et al. 2014a). In the facultative mixotroph, CCMP2951 mitochondrial respiration was negligible as an electron sink under low-light intensities and the overflow mechanism at higher light intensities mainly relied on alternative oxidase, which does not contribute to the proton gradient for ATP production (Vanlerberghe and McIntosh 1997). Hence, in contrast to the obligate mixotroph, mitochondrial respiration is not required as an integral part of photosynthetic electron transport in the facultative mixotroph.

Differences in phenotypic plasticity between the two isolates studied here are further reflected in their responses to super-saturating irradiances. In the obligate mixotroph, growth rates were reduced under long-term exposure to high light despite the maintenance of high electron transport rates during short-term exposure. This indicates a downstream limitation to electron transport that could not be counteracted by photoacclimation. The lower content of the photoprotective pigments carotene, and diadinoxanthin in the obligate mixotroph, relative to the facultative mixotroph, might contribute to its higher susceptibility to photoinhibition. The light-induced de-epoxidized form of diadinoxanthin, diatoxanthin, is responsible for some forms of NPQ in other stramenopiles, specifically diatoms (Arsalane et al. 1994). However, we did not detect this pigment in either *Ochromonas* isolate, consistent with its absence in other chrysophytes (Lichtlé et al. 1995, Tanabe et al. 2011). Differences in VAZ pool size might underlie the higher NPQ capacity in CCMP2951, but cannot fully explain the large difference between isolates. These might be due to other components involved in NPQ such as the ancient light harvesting related protein (LHCSR and LHX) found in diatoms and green algae (Peers et al. 2009, Bailleul et al. 2010, Guo et al. 2018). In addition, the formation of a pH gradient across the thylakoid membrane is required for the induction of NPQ. In CCMP1393, a slight NPQ response is already present in darkness, indicative of a pH gradient formed through chlororespiration (Jakob et al. 1999). If the close interaction between plastids and mitochondria in this isolate supports a pH gradient across the thylakoid membrane independently of light, a strong NPQ response might not be beneficial as it could restrict photosynthesis at low-light intensities.

The two mixotrophic strategies described here likely reflect adaptation to different niches, although the specific competitive advantages gained within complex communities is difficult to assess and the environmental distributions of mixotrophic strategies remain largely unstudied. A first assessment of the biogeography of mixotrophs revealed a gap in information regarding non-dinoflagellate constitutive mixotrophs (Leles et al. 2019), such as the chrysophytes studied here. In modeling studies, constitutive mixotrophs are typically considered to be primarily autotrophic, supplementing their nutrition by ingestion of prey if either light or nutrients become limiting and thus have an advantage under nutrient limitation (Leles et al. 2018). This is a strategy, for example, found in prymnesiophytes and some dinoflagellates (Hansen and Hjorth 2002, Hansen 2011). However, the spectrum of constitutive mixotrophs, ranging from preferentially heterotrophic to obligately mixotrophic is less commonly addressed. In a similar manner to which primarily autotrophic mixotrophs have an advantage competing for nutrients against non-phagocytotic photoautotrophs in nutrient limiting conditions, primarily heterotrophic mixotrophs could have an advantage over purely heterotrophic taxa at low prey availability, if sufficient light is available (Tittel et al. 2003, Fischer et al. 2017). Both types of mixotrophic strategies could thus be advantageous in oligotrophic environments. Obligate mixotrophy has been implemented in modeling studies in the form of kleptoplasty, where the capacity of a heterotrophic protist to photosynthesize depends on its ingestion of autotrophic prey (Mitra et al. 2016). Although based on different underlying physiology, kleptoplastic protists dominated predicted plankton biomass in a nutrient-limited scenario (Leles et al. 2018), hinting at the success of obligate mixotrophs in oligotrophic waters. From our results, the narrow range of environmental conditions that permit growth of the obligate mixotroph might seem disadvantageous, but this strategy is likely efficient in stable environments with low-resource availability. Additionally, while the facultative mixotroph still reached a higher percentage of its maximum growth rate under light limitation, this advantage

might disappear under low but stable availability of light and prey, when close integration of photosynthesis and heterotrophy in the obligate mixotroph presumably preserves resources. Moreover, export of photosynthetically derived electrons to the mitochondrial respiratory chain, even under low-light conditions, could reduce the need to respire ingested carbon and therefore allow higher carbon assimilation efficiencies. Obligate mixotrophy could hence represent a specialization for stable resource-limited environments such as the oligotrophic oceans, while facultative mixotrophy would be more advantageous under fluctuating conditions as found in shallower coastal regions.

The opposite responses to environmental drivers observed in the two marine *Ochromonas* species studied here suggest that even closely related mixotrophic protists will respond differently to changing ocean conditions with differing consequences for carbon cycling through marine microbial food webs. For instance, the nutritional balance of mixotrophs might directly be affected by warming with a shift toward a more heterotrophic nutrition at higher temperatures (Wilken et al. 2013, Worden et al. 2015). Such a shift would be more likely in facultative mixotrophs that have greater nutritional flexibility than in obligate mixotrophs which have a close interdependency of photosynthesis and heterotrophy. Further, expansion of oligotrophic regions as oceans warm (Polovina et al. 2008) may provide conditions favoring the resource efficient strategy, i.e., obligate mixotrophy. Understanding the physiological basis of different mixotrophic strategies in a broader assortment of environmentally relevant models will help to predict their respective biogeography and contributions to food web dynamics and carbon cycling in the future oceans.

## ACKNOWLEDGMENTS

We thank E. Ruby for providing the *Vibrio fischeri* strain, F. Chavez for access to a radioactive isotope lab, T. Pennington for help with establishing the carbon fixation protocol, D. Klimov for help with FRRf-setup, and M. Hamilton for help with sampling. Finally, we thank R. Massana for cosponsoring SW's Marie Curie Postdoctoral Fellowship. This work was supported by grants from the Department of Energy (DOE-DE-SC0004765) and Gordon and Betty Moore Foundation (GBMF3307 and GBMF3788) to AZW and SW was supported largely by a Postdoctoral Fellowship from the European Union's Seventh Framework Programme under the *Marie* Skłodowska-*Curie* grant agreement No 626182.

## AUTHOR CONTRIBUTIONS

AZW and SW planned and designed the research; SW performed experiments and analyzed physiology data; and CJC performed sequencing and phylogenetic analysis. SW drafted the manuscript with input from AZW and additional edits from CJC.

## REFERENCES

Allen, A. E., LaRoche, J., Maheswari, U., Lommer, M., Schauer, N., Lopez, P. J., Finazzi, G., Fernie, A. R. & Bowler, C. 2008. Whole-cell response of the pennate diatom *Phaeodactylum tricornutum* to iron starvation. *Proc. Natl. Acad. Sci. USA* 105:10438–43.

Andersen, K. H., Aksnes, D. L., Berge, T., Fiksen, Ø. & Visser, A. 2015. Modelling emergent trophic strategies in plankton. *J. Plankton Res.* 37:862–8.

Andersson, A., Falk, S., Samuelsson, G. & Hagström, Å. 1989. Nutritional characteristics of a mixotrophic nanoflagellate, *Ochromonas* sp. *Microb. Ecol.* 17:251–62.

Arsalane, W., Rousseau, B. & Duval, J. 1994. Influence of the pool size of the xanthophyll cycle on the effects of light stress in a diatom: Competition between photoprotection and photoinhibition. *Photochem. Photobiol.* 60:237–43.

Azam, F., Fenchel, T., Field, J. G., Gray, J. S., Meyerreil, L. A. & Thingstad, F. 1983. The ecological role of water-column microbes in the sea. *Mar. Ecol. Prog. Ser.* 10:257–63.

Bailey, S., Melis, A., Mackey, K. R. M., Cardol, P., Finazzi, G., van Dijken, G., Berg, G. M., Arrigo, K., Shrager, J. & Grossman, A. 2008. Alternative photosynthetic electron flow to oxygen in marine *Synechococcus*. *Biochim. Biophys. Acta BBA Bioenerg.* 1777:269–76.

Bailleul, B., Berne, N., Murik, O., Petroutsos, D., Prihoda, J., Tanaka, A., Villanova, V., et al. 2015. Energetic coupling between plastids and mitochondria drives $CO_2$ assimilation in diatoms. *Nature* 524:366–9.

Bailleul, B., Rogato, A., de Martino, A., Coesel, S., Cardol, P., Bowler, C., Falciatore, A. & Finazzi, G. 2010. An atypical member of the light-harvesting complex stress-related protein family modulates diatom responses to light. *Proc. Natl. Acad. Sci. USA* 107:18214–9.

Berge, T., Chakraborty, S., Hansen, P. J. & Andersen, K. H. 2017. Modeling succession of key resource-harvesting traits of mixotrophic plankton. *ISME J.* 11:212–23.

Bird, D. F. & Kalff, J. 1986. Bacterial grazing by planktonic lake algae. *Science* 231:493–5.

Boenigk, J., Pfandl, K., Stadler, P. & Chatzinotas, A. 2005. High diversity of the '*Spumella*-like' flagellates – an investigation based on the SSU rRNA gene sequences of isolates from habitats located in six different geographic regions. *Environ. Microbiol.* 7:685–97.

del Campo, J. & Massana, R. 2011. Emerging diversity within chrysophytes, choanoflagellates and bicosoecids based on molecular surveys. *Protist* 162:435–48.

Caron, D. A., Porter, K. G. & Sanders, R. W. 1990. Carbon, nitrogen, and phosphorus budgets for the mixotrophic phytoflagellate *Poterioochromonas malhamensis* (chrysophyceae) during bacterial ingestion. *Limnol. Oceanogr.* 35:433–43.

Caron, D. A., Sanders, R. W., Lim, E. L., Marrase, C., Amaral, L. A., Whitney, S., Aoki, R. B. & Porter, K. G. 1993. Light-dependent phagotrophy in the freshwater mixotrophic chrysophyte *Dinobryon cylindricum*. *Microb. Ecol.* 25:93–111.

Castresana, J. 2000. Selection of conserved blocks from multiple alignments for their use in phylogenetic analysis. *Mol. Biol. Evol.* 17:540–52.

Cuvelier, M. L., Allen, A. E., Monier, A., McCrow, J. P., Messie, M., Tringe, S. G., Woyke, T. et al. 2010. Targeted metagenomics and ecology of globally important uncultured eukaryotic phytoplankton. *Proc. Natl. Acad. Sci. USA* 107:14679–84.

Cuvelier, M. L., Guo, J., Ortiz, A. C., van Baren, M. J., Akram Tariq, M., Partensky, F. & Worden, A. Z. 2017. Responses of the picoprasinophyte *Micromonas commoda* to light and ultraviolet stress. *PLoS ONE* 12:e0172135.

Dunn, A. K., Millikan, D. S., Adin, D. M., Bose, J. L. & Stabb, E. V. 2006. New rfp- and pES213-derived tools for analyzing symbiotic *Vibrio fischeri* reveal patterns of infection and lux expression in situ. *Appl. Environ. Microbiol.* 72:802–10.

Estep, K. W., Davis, P. G., Keller, M. D. & Sieburth, J. M. 1986. How important are oceanic algal nanoflagellates in bacterivory? *Limnol. Oceanogr.* 31:646–50.

Field, C. B., Behrenfeld, M. J., Randerson, J. T. & Falkowski, P. 1998. Primary production of the biosphere: Integrating terrestrial and oceanic components. *Science* 281:237–40.

Fischer, R., Giebel, H. A., Hillebrand, H. & Ptacnik, R. 2017. Importance of mixotrophic bacterivory can be predicted by light and loss rates. *Oikos* 126:713–22.

Flöder, S., Hansen, T. & Ptacnik, R. 2006. Energy-dependent bacterivory in *Ochromonas minima* – a strategy promoting the use of substitutable resources and survival at insufficient light supply. *Protist* 157:291–302.

Flynn, K. J. & Mitra, A. 2009. Building the "perfect beast": modelling mixotrophic plankton. *J. Plankton Res.* 31:965–92.

Flynn, K. J., Stoecker, D. K., Mitra, A., Raven, J. A., Glibert, P. M., Hansen, P. J., Graneli, E. & Burkholder, J. M. 2013. Misuse of the phytoplanktonzooplankton dichotomy: the need to assign organisms as mixotrophs within plankton functional types. *J. Plankton Res.* 35:3–11.

Graf, J., Dunlap, P. V. & Ruby, E. G. 1994. Effect of transposon-induced motility mutations on colonization of the host light organ by Vibrio fischeri. *J. Bacteriol.* 176:6986–91.

Grossmann, L., Bock, C., Schweikert, M. & Boenigk, J. 2016. Small but manifold – hidden diversity in '*Spumella*-like flagellates'. *J. Euk. Microbiol.* 63:419–39.

Guindon, S., Dufayard, J. F., Lefort, V., Anisimova, M., Hordijk, W. & Gascuel, O. 2010. New algorithms and methods to estimate maximum-likelihood phylogenies: assessing the performance of PhyML 3.0. *Systematic Biol.* 59:307–21.

Guo, J., Wilken, S., Jimenez, V., Choi, C. J., Ansong, C., Dannebaum, R., Sudek, L. et al. 2018. Specialized proteomic responses and an ancient photoprotection mechanism sustain marine green algal growth during phosphate limitation. *Nature Microbiol.* 3:781–90.

Hansen, P. J. 2011. The role of photosynthesis and food uptake for the growth of marine mixotrophic dinoflagellates. *J. Eukaryot. Microbiol.* 58:203–14.

Hansen, P. J. & Hjorth, M. 2002. Growth and grazing responses of *Chrysochromulina ericina* (Prymnesiophyceae): the role of irradiance, prey concentration and pH. *Mar. Biol.* 141:975–83.

Hartmann, M., Grob, C., Tarran, G. A., Martin, A. P., Burkill, P. H., Scanlan, D. J. & Zubkov, M. V. 2012. Mixotrophic basis of atlantic oligotrophic ecosystems. *Proc. Natl. Acad. Sci. USA* 109:5756–60.

Hartmann, M., Zubkov, M. V., Scanlan, D. J. & Lepère, C. 2013. In situ interactions between photosynthetic picoeukaryotes and bacterioplankton in the atlantic ocean: evidence for mixotrophy. *Environ. Microbiol. Reports* 5:835–40.

Havskum, H. & Hansen, A. S. 1997. Importance of pigmented and colourless nano-sized protists as grazers on nanoplankton in a phosphate-depleted Norwegian fjord and in enclosures. *Aquat. Microb. Ecol.* 12:139–51.

Heinbokel, J. F. 1978. Studies on the functional role of tintinnids in the southern California bight I. Grazing and growth rates in laboratory cultures. *Mar. Biol.* 47:177–89.

Jakob, T., Goss, R. & Wilhelm, C. 1999. Activation of diadinoxanthin de-epoxidase due to a chlororespiratory proton gradient in the dark in the diatom *Phaeodactylum tricornutum*. *Plant Biol.* 1:76–82.

Jardillier, L., Zubkov, M. V., Pearman, J. & Scanlan, D. J. 2010. Significant $CO_2$ fixation by small prymnesiophytes in the subtropical and tropical northeast Atlantic ocean. *ISME J.* 4:1180–92.

Jeong, H. J., Yoo, Y. D., Kim, J. S., Seong, K. A., Kang, N. S. & Kim, T. H. 2010. Growth, feeding and ecological roles of mixotrophic and heterotrophic dinoflagellates in marine planktonic food webs. *Ocean Sci. J.* 45:65–91.

Katoh, K. & Standley, D. M. 2013. MAFFT multiple sequence alignment software version 7: improvements in performance and usability. *Mol. Biol. Evol.* 30:772–80.

Keeling, P. J. 2013. The number, speed, and impact of pastid endosymbioses in eukaryotic evolution. *Annu. Rev. Plant Biol.* 64:583–607.

Keeling, P. J., Burki, F., Wilcox, H. M., Allam, B., Allen, E. E., Amaral-Zettler, L. A., Armbrust, E. V. et al. 2014. The Marine Microbial Eukaryote Transcriptome Sequencing Project (MMETSP): illuminating the functional diversity of eukaryotic life in the oceans through transcriptome sequencing. *PLoS Biol.* 12:e1001889.

Keller, M. D., Selvin, R. C., Claus, W. & Guillard, R. R. L. 1987. Media for the culture of oceanic ultraphytoplankton. *J. Phycol.* 23:633–8.

Kimura, B. & Ishida, Y. 1989. Phospholipid as a growth factor of *Uroglena americana*, a red tide chrysophyceae in Lake Biwa. *Nippon Suisan Gakkaishi* 55:799–804.

Kirkham, A. R., Lepère, C., Jardillier, L. E., Not, F., Bouman, H., Mead, A. & Scanlan, D. J. 2013. A global perspective on marine photosynthetic picoeukaryote community structure. *ISME J.* 7:922–36.

Kolber, Z. S., Prasil, O. & Falkowski, P. G. 1998. Measurements of variable chlorophyll fluorescence using fast repetition rate techniques: Defining methodology and experimental protocols. *Biochim. Biophys. Acta BBA Bioenerg.* 1367:88–106.

Lane, C. E. & Archibald, J. M. 2008. The eukaryotic tree of life: endosymbiosis takes its TOL. *Trends Ecol. Evol.* 23:268–75.

Leles, S. G., Mitra, A., Flynn, K. J., Tillmann, U., Stoecker, D., Jeong, H. J., Burkholder, J. et al. 2019. Sampling bias misrepresents the biogeographical significance of constitutive mixotrophs across the global oceans. *Global Ecol. Biogeogr.* 28:418–28.

Leles, S. G., Polimene, L., Bruggeman, J., Blackford, J., Ciavatta, S., Mitra, A. & Flynn, K. J. 2018. Modelling mixotrophic functional diversity and implications for ecosystem function. *J. Plankton Res.* 40:627–42.

Lepère, C., Vaulot, D. & Scanlan, D. J. 2009. Photosynthetic picoeukaryote community structure in the South East Pacific Ocean encompassing the most oligotrophic waters on Earth. *Environ. Microbiol.* 11:3105–17.

Lichtlé, C., Arsalane, W., Duval, J. C. & Passaquet, C. 1995. Characterization of the light-harvesting complex of *Giraudyopsis stellifer* (Chrysophyceae) and effects of light stress. *J. Phycol.* 31:380–7.

Lie, A. A. Y., Liu, Z., Terrado, R., Tatters, A. O., Heidelberg, K. B. & Caron, D. A. 2018. A tale of two mixotrophic chrysophytes – insights into the metabolisms of two *Ochromonas* species (Chrysophyceae) through a comparison of gene expression. *PLoS ONE* 13:e0192439.

MacIntyre, H. L., Kana, T. M., Anning, T. & Geider, R. J. 2002. Photoacclimation of photosynthesis irradiance response curves and photosynthetic pigments in microalgae and cyanobacteria. *J. Phycol.* 38:17–38.

McDonald, S.M., Plant, J.N. & Worden, A.Z. 2010. The mixed lineage nature of nitrogen transport and assimilation in marine eukaryotic phytoplankton: a case study of *Micromonas*. *Mol. Biol. Evol.* 27: 2268-83.

Milligan, A. J., Halsey, K. H. & Behrenfeld, M. J. 2015. Advancing interpretations of $^{14}C$-uptake measurements in the context of phytoplankton physiology and ecology. *J. Plankton Res.* 37:692–8.

Millikan, D. S. & Ruby, E. G. 2003. FlrA, a $\sigma^{54}$-dependent transcriptional activator in *Vibrio fischeri*, is required for motility and symbiotic light-organ colonization. *J. Bacteriol.* 185:3547–57.

Mitra, A., Flynn, K. J., Burkholder, J. M., Berge, T., Calbet, A., Raven, J. A., Granéli, E. et al. 2014. The role of mixotrophic protists in the biological carbon pump. *Biogeosciences* 11:995–1005.

Mitra, A., Flynn, K. J., Tillmann, U., Raven, J. A., Caron, D., Stoecker, D. K., Not, F. et al. 2016. Defining planktonic protist functional groups on mechanisms for energy and nutrient acquisition - incorporation of diverse mixotrophic strategies. *Protist* 167:106–20.

Moon-van der Staay, S. Y., De Wachter, R. & Vaulot, D. 2000. Oceanic 18S rDNA sequences from picoplankton reveal unsuspected eukaryotic diversity. *Nature* 409:607–10.

Orsi, W. D., Wilken, S., del Campo, J., Heger, T., James, E., Richards, T. A., Keeling, P. J., Worden, A. Z. & Santoro, A.

E. 2018. Identifying protist consumers of photosynthetic picoeukaryotes in the surface ocean using stable isotope probing. *Environ. Microbiol.* 20:815–27.
Pålsson, C. & Daniel, C. 2004. Effects of prey abundance and light intensity on nutrition of a mixotrophic flagellate and its competitive relationship with an obligate heterotroph. *Aquat. Microb. Ecol.* 36:247–56.
Peers, G., Truong, T. B., Ostendorf, E., Busch, A., Elrad, D., Grossman, A. R., Hippler, M. & Niyogi, K. K. 2009. An ancient light-harvesting protein is critical for the regulation of algal photosynthesis. *Nature* 462:518–21.
Pennington, J. T. & Chavez, F. P. 2000. Seasonal fluctuations of temperature, salinity, nitrate, chlorophyll and primary production at station H3/M1 over 1989–1996 in Monterey bay, California. *Deep Sea Res. Part 2 Top. Stud. Oceanogr.* 47:947–73.
Polovina, J. J., Howell, E. A. & Abecassis, M. 2008. Ocean's least productive waters are expanding. *Geophys. Res. Lett.* 35:L03618.
Pomeroy, L. R. 1974. The ocean's food web, a changing paradigm. *Bioscience* 24:499–504.
Pruesse, E., Quast, C., Knittel, K., Fuchs, B. M., Ludwig, W., Peplies, J. & Glockner, F. O. 2007. SILVA: a comprehensive online resource for quality checked and aligned ribosomal RNA sequence data compatible with ARB. *Nucl. Acids Res.* 35:7188–96.
Ronquist, F., Teslenko, M., van der Mark, P., Ayres, D. L., Darling, A., Hohna, S., Larget, B., Liu, L., Suchard, M. A. & Huelsenbeck, J. P. 2012. MrBayes 3.2: efficient Bayesian phylogenetic inference and model choice across a large model space. *Systematic Biol.* 61:539–42.
Rothhaupt, K. O. 1996. Utilization of substitutable carbon and phosphorus sources by the mixotrophic chrysophyte *Ochromonas* sp. *Ecology* 77:706–15.
Rothhaupt, K. O. 1997. Nutrient turnover by freshwater bacterivorous flagellates: Differences between a heterotrophic and a mixotrophic chrysophyte. *Aquat. Microb. Ecol.* 12:65–70.
Sanders, R. W., Berninger, U. G., Lim, E. L., Kemp, P. F. & Caron, D. A. 2000. Heterotrophic and mixotrophic nanoplankton predation on picoplankton in the Sargasso Sea and on George's Bank. *Mar. Ecol. Prog. Ser.* 192:103–18.
Sanders, R. W., Porter, K. G. & Caron, D. A. 1990. Relationship between phototrophy and phagotrophy in the mixotrophic chrysophyte *Poterioochromonas malhamensis*. *Microb. Ecol.* 19:97–109.
Schuback, N., Schallenberg, C., Duckham, C., Maldonado, M. T. & Tortell, P. D. 2015. Interacting effects of light and iron availability on the coupling of photosynthetic electron transport and $CO_2$-assimilation in marine phytoplankton. *PLoS ONE* 10:e0133235.
Selosse, M. A., Charpin, M. & Not, F. 2017. Mixotrophy everywhere on land an in water: the grand écart hypothesis. *Ecol. Let.* 20:246–63.
Stabb, E. V., Reich, K. A. & Ruby, E. G. 2001. *Vibrio fischeri* genes hvnA and hvnB encode secreted NAD(+)-glycohydrolases. *J. Bacteriol.* 183:309–17.
Stamatakis, A. 2014. RAxML version 8: a tool for phylogenetic analysis and post-analysis of large phylogenies. *Bioinformatics* 30:1312–3.
Stoecker, D. K. 1998. Conceptual models of mixotrophy in planktonic protists and some ecological and evolutionary implications. *Eur. J. Protistol.* 34:281–90.
Stoecker, D. K. & Michaels, A. E. 1991. Respiration, photosynthesis and carbon metabolism in planktonic ciliates. *Mar. Biol.* 108:441–7.
Tanabe, Y., Shitara, T., Kashino, Y., Hara, Y. & Kudoh, S. 2011. Utilizing the effective xanthophyll cycle for blooming of *Ochromonas smithii* and *O. itoi* (Chrysophyceae) on the snow surface. *PLoS ONE* 6:e14690.
Tittel, J., Bissinger, V., Zippel, B., Gaedke, U., Bell, E., Lorke, A. & Kamjunke, N. 2003. Mixotrophs combine resource use to outcompete specialists - implications for aquatic food webs. *Proc. Natl. Acad. Sci. USA* 100:12776–81.
Unrein, F., Gasol, J. M., Not, F., Forn, I. & Massana, R. 2014. Mixotrophic haptophytes are key bacterial grazers in oligotrophic coastal waters. *ISME J.* 8:164–76.
Unrein, F., Massana, R., Alonso-Saez, L. & Gasol, J. M. 2007. Significant year-round effect of small mixotrophic flagellates on bacterioplankton in an oligotrophic coastal system. *Limnol. Oceanogr.* 52:456–69.
Van Heukelem, L. & Thomas, C. S. 2001. Computer-assisted high-performance liquid chromatography method development with applications to the isolation and analysis of phytoplankton pigments. *J. Chromatogr. A* 910:31–49.
Vanlerberghe, G. C. & McIntosh, L. 1997. Alternative oxidase: From gene to function. *Annu. Rev. Plant Physiol. Plant Mol. Biol.* 48:703–34.
Ward, B. A. & Follows, M. J. 2016. Marine mixotrophy increases trophic transfer efficiency, mean organism size, and vertical carbon flux. *Proc. Natl. Acad. Sci. USA* 113:2958–63.
Webb, W. L., Newton, M. & Starr, D. 1974. Carbon dioxide exchange of *Alnus rubra*. *Oecologia* 17:281–91.
Wilken, S., Huisman, J., Naus-Wiezer, S. & Van Donk, E. 2013. Mixotrophic organisms become more heterotrophic with rising temperature. *Ecology Lett.* 16:225–33.
Wilken, S., Schuurmans, J. M. & Matthijs, H. C. P. 2014a. Do mixotrophs grow as photoheterotrophs? photophysiological acclimation of the chrysophyte *Ochromonas danica* after feeding. *New Phytol.* 204:882–9.
Wilken, S., Verspagen, J. M. H., Naus-Wiezer, S., Van Donk, E. & Huisman, J. 2014b. Comparison of predator-prey interactions with and without intraguild predation by manipulation of the nitrogen source. *Oikos* 123:423–32.
Worden, A. Z. 2006. Picoeukaryote diversity in coastal waters of the Pacific Ocean. *Aquat. Microb. Ecol.* 43:165–75.
Worden, A. Z., Follows, M. J., Giovannoni, S. J., Wilken, S., Zimmerman, A. E. & Keeling, P. J. 2015. Rethinking the marine carbon cycle: Factoring in the multifarious lifestyles of microbes. *Science* 347:1257594.
Worden, A. Z., Lee, J. H., Mock, T., Rouzé, P., Simmons, M. P., Aerts, A. L., Allen, A. E. et al. 2009. Green evolution and dynamic adaptations revealed by genomes of the marine picoeukaryotes *Micromonas*. *Science* 324:268–72.
Worden, A. Z., Seidel, M., Smriga, S., Wick, A., Malfatti, M., Bartlett, D. & Azam, F. 2006. Trophic regulation of *Vibrio cholera* in coastal marine waters. *Environ. Microbiol.* 8:21–9.

## Supporting Information

Additional Supporting Information may be found in the online version of this article at the publisher's web site:

**Figure S1.** Abundances of *Ochromonas* and the bacterial prey *Vibrio fischeri* in semi-continuous cultures of the two *Ochromonas* isolates with or without daily prey-amendments.

**Figure S2.** Forward-angle light scatter (FALS) of *Ochromonas* isolates under prey-amended and prey-deplete conditions.

**Figure S3.** Molar ratio of diadinoxanthin content relative to chlorophyll *a* in the two *Ochromonas* isolates under prey-amended and prey-deplete conditions.